



Noble gases and coupled heat/fluid flow modeling for evaluating hydrogeologic conditions of volcanic island aquifers

Victor M. Heilweil^{a,*}, Richard W. Healy^b, Robert N. Harris^c

^aU.S. Geological Survey, Utah Water Science Center, Salt Lake City, Utah, United States

^bU.S. Geological Survey, National Research Program, Lakewood, Colorado, United States

^cU.S. Oregon State University, College of Earth, Oceanic, and Atmospheric Sciences, Corvallis, Oregon, United States

ARTICLE INFO

Article history:

Received 10 April 2012

Received in revised form 5 July 2012

Accepted 12 July 2012

Available online 22 July 2012

This manuscript was handled by Corrado Corradini, Editor-in-Chief, with the assistance of Diana M. Allen, Associate Editor

Keywords:

Groundwater recharge

Cape Verde Islands

Coupled heat/fluid flow simulations

Volcanic island aquifer

Noble-gas thermometry

SUMMARY

Understanding groundwater conditions in the upland parts of volcanic island aquifers is critical for sustainable groundwater development in these resource-limited environments. Yet groundwater conditions in such settings are generally difficult to characterize because of sparse well drilling (high cost and/or limited access). Information needed for resource evaluation includes upland depth to water, recharge rate, and aquifer permeability. In this study, noble-gas recharge temperatures and coupled heat/fluid flow modeling are used to indirectly infer these groundwater conditions. Mosteiros Basin on Fogo Island of the Cape Verde archipelago was selected as a representative volcanic island aquifer. Simulation results are calibrated to water-table altitude and temperature data, along with indirect information provided by noble and dissolved gases. Results of numerical modeling are most sensitive to recharge rates and hydraulic conductivity, less sensitive to basal heat flux, and not sensitive to porosity and thermal conductivity. Simulation results show that only a relatively narrow range of combined recharge values (12–25% of precipitation) and hydraulic conductivity (10^{-8} – 10^{-7} m s⁻¹) is consistent with observed data. The simulated recharge of 3–6 million cubic meters per year (Mm³ yr⁻¹) is much higher than measured discharge from the basin (0.25 Mm³ yr⁻¹), indicating the occurrence of significant amounts of submarine groundwater discharge. The modeling results suggest a very deep upland water table located 600–1000 m beneath the floor of the central caldera, although the water table becomes more shallow and accessible towards the coast. Perhaps most significant is the dominant role that modest amounts of recharge (mean rates of 70–140 mm yr⁻¹) plays in decreasing the geothermal gradient, resulting in relatively cool temperatures in the deep vadose and at the water table. Noble-gas recharge temperatures, constrained by numerical simulation results, range from about 15 to 22 °C and indicate a large water-table temperature lapse of about –15 °C/km, much steeper than typical adiabatic lapse rates.

Published by Elsevier B.V.

1. Introduction

The development of volcanic island groundwater resources is typically limited by the tradeoff between developing lowland areas (shallow water table but susceptible to contamination) and upland areas, where salt-water intrusion is unlikely but accessibility due to steep terrain and a deep water table makes production difficult. Volcanic island aquifers can be broadly classified as either (1) continuous systems with deep basal water tables in upland areas connected to coastal aquifers or (2) disconnected systems with shallow upland water tables, isolated from coastal aquifers by low permeability volcanic structures. Such shallow upland aquifers may be more accessible to development, but productivity of supply wells may be limited. With both types of groundwater systems,

information on groundwater conditions in the upland parts of volcanic island watersheds is important for evaluating the potential for future groundwater development. In particular, an improved understanding of upland water-table geometry, permeability, and recharge is critical, especially where coastal aquifers are already heavily impacted by contamination and (or) saltwater intrusion.

In unconfined aquifers within mountainous terrain, water-table altitude is predominantly controlled by infiltration rate and permeability, and to a lesser extent, by factors such as topography, basal heat flow, and thermal conductivity (Forster and Smith, 1988). Water-table depth information within steep mountainous terrain is scarce and groundwater processes in such regimes are generally poorly understood (Manning and Caine, 2007); this is particularly true for active volcanoes (Hurwitz et al., 2003; Ingebritsen et al., 2010). Groundwater noble-gas measurements from wells and springs at distal discharge locations, however, can provide upland water-table temperature and altitude information (Mazor, 1991;

* Corresponding author. Tel.: +1 801 908 5042; fax: +1 801 908 5001.

E-mail address: heilweil@usgs.gov (V.M. Heilweil).

Aeschbach-Hertig et al., 1999; Manning and Solomon, 2003; Manning, 2011). Temperature regimes within active volcanic aquifer systems can be strongly affected by groundwater circulation; this combined fluid and heat flow is described by coupled groundwater flow and heat transport equations (Ingebritsen et al., 2006). Coupled flow and thermal modeling, aided by groundwater temperature information, has been used in numerous studies to estimate infiltration rates and hydraulic properties, often elucidating perturbations of the geothermal gradient caused by regional groundwater flow (Anderson, 2005). Whereas many investigations have examined high-temperature fluid circulation associated with magmatic hydrothermal systems in volcanic edifices (Ingebritsen et al., 2010), lesser attention has been given to coupled flow and heat transport in adjacent aquifer systems from the perspective of water resources development.

In this study, we use an innovative approach by combining measured/noble-gas-derived water-temperature and coastal water-table altitude data with coupled groundwater flow and heat transport modeling to provide information on recharge rates, aquifer permeability, and water-table depths in the upland areas of active volcanic-island aquifers. Direct information on upland water-table depths on volcanic islands is often difficult and costly to obtain; the cost-effective indirect approach taken in this study can provide useful insights to these complex hydrogeologic systems.

1.1. Volcanic island hydrogeology

Previous studies have shown that groundwater temperature distribution within active volcanoes is dependent upon the amount of heat supplied by the underlying magma, recharge volumes, and permeability structures (Hurwitz et al., 2002). Groundwater flow and thermal regimes of magmatic hydrothermal systems including active volcanoes have increasingly been investigated with numerical models (Ingebritsen et al., 2010). Separate hydrologic and thermal models were developed to evaluate groundwater circulation and interaction with hot magmatic fluids within the active Piton de la Fournaise volcano on the Indian Ocean Island of Reunion (Violette et al., 1997). More recently, coupled groundwater and heat transport modeling of a continental volcano-hydrothermal system found that water-table altitude and temperature are predominantly controlled by hydraulic properties, recharge rate and temperatures, and basal heat flux (Hurwitz et al., 2003).

Because coupled heat and fluid flow models of volcanic islands and knowledge of the hydraulic and thermal rock properties are rare in general and Cape Verde specifically, we review these properties. Information was compiled from studies at active oceanic volcano-hydrothermal systems worldwide. A wide range in magnitudes of saturated hydraulic conductivity (10^{-12} – 10^0 m s⁻¹) has been reported for volcanic island shield basalts (Appendix A). Reductions in permeability, caused by intrusive igneous dikes, hydrothermal alteration, low-porosity non-fractured basalt layers, or massive post-shield basalt deposits have been reported for several volcanic island aquifer systems. Dikes, typically having a near-vertical orientation and thickness of less than 3 m, can number more than 600 per kilometer in the center of a dike complex and comprise more than 10% of the total rock volume (Takasaki and Mink, 1985). These structures are generally less permeable than the basalts they intrude. Saturated hydraulic conductivity values reported for dike complexes of Oahu were as much as four orders of magnitude lower than for dike-free zones (Hunt, 1996; Rotzoll et al., 2007). Ingebritsen and Scholl (1993) reported much lower hydraulic conductivity for deeply buried (>1 km) basalts of the Kilauea volcanic rift zone on Hawaii compared to surficial basalt flows, attributed to either pervasive intrusion of less-permeable dikes and (or) hydrothermal alteration. Saturated hydraulic

conductivity values about 1–4 orders of magnitude less than shield building-stage basaltic aquifers were reported for post-shield and rejuvenated-stage basin-filling basalts of the southern Lihue Basin on the island of Kauai, Hawaii (Gingerich, 1999; Izuka and Gingerich, 2003). For the Teide Volcano of Tenerife (Canary Islands), a high degree of anisotropy is due to shield volcano layering and alternation of low permeability non-fractured dike-intruded basalts with more permeable fractured basalts (Valentin et al., 1990).

Reported total porosity values for basalt vary over almost half an order of magnitude. Porosity values for Hawaiian basalts range from about 0.05 to more than 0.5 (Mink and Lau, 1980). Similar values of 0.05 and 0.5 (for the basal unit and upper basalt aquifer, respectively) were used for thermal modeling of the Piton de la Fournaise volcano (Violette et al., 1997); smaller values of 0.01–0.25 were used in coupled flow/thermal simulations of a hypothetical Cascade Mountains (continental) stratovolcano system (Hurwitz et al., 2003).

Groundwater recharge is influenced by several factors including climate, geology, topography, hydrology, vegetation, and land use (Healy, 2010). In warm (rainfall-rather than snowmelt-dominated) climates, the partitioning of precipitation between runoff, evapotranspiration, and groundwater recharge is controlled by a combination of surficial permeability (soil/bedrock), soil–water storage, topographic slope, bare-soil evaporation and plant transpiration (Flint et al., 2004). Recharge estimates for volcanic island watersheds are primarily derived from water-budget models. Recharge to the Piton de la Fournaise volcano is estimated to be 57% of precipitation based on a coupled surface-water and groundwater model (Violette et al., 1997). In the Hawaiian Islands, mean estimated recharge ranges from about 10% to 80% of precipitation (Engott, 2011; Gingerich and Oki, 2000; Izuka et al., 2005; Oki, 2005). The highest recharge rates are generally located in wetter areas with highly permeable surficial deposits, whereas lower rates were found in warmer and drier areas.

Reported water-table elevations for volcanic oceanic island aquifers range from low-altitude, low-gradient regional water tables that are located near sea level at great depth beneath the island's interior to high-altitude, high-gradient water tables (Liu et al., 1983; Jackson and Lenat, 1989; Gingerich and Oki, 2000). Low-altitude water tables in Hawaii were first reported by Meinzer (1930) and termed “basal ground-water” (Fig. 1). While such basal groundwater conditions are often encountered (Hunt, 1996), high-altitude water tables have been documented in many volcanic island aquifer systems. Particular examples include a water-table altitude of more than 600 m measured in a research borehole drilled beneath the summit of the Kilauea volcano on the island of Hawaii (Keller et al., 1979); regional groundwater-table altitudes approaching 1200 m in the volcanic aquifer system of Madeira Island (Prada et al., 2005); and regional spring altitudes of up to 800 m in the Fautaua Basin on the flanks of a shield volcano in Tahiti (Hildenbrand et al., 2005). Groundwater studies of Hawaii (Macdonald et al., 1983; Oki et al., 1999) were the first to introduce the conceptual model of a regionally-connected high-altitude water table with stair-step water-table compartmentalization caused by low permeability vertical dikes acting as horizontal flow barriers (Fig. 1). Examples include dike impounded groundwater in the Koolau Volcano rift zone on the island of Oahu (Takasaki and Mink, 1985; Oki, 2005) and in the interior of West Maui Mountain (Engott and Vana, 2007). While high-altitude regional water tables are typically associated with dike-impounded conditions, a regional water table in the Lihue Basin of Kauai occurs hundreds of meters above sea level within a few kilometers of the coast, attributed to thick low-permeability basalts (Izuka and Gingerich, 2003).

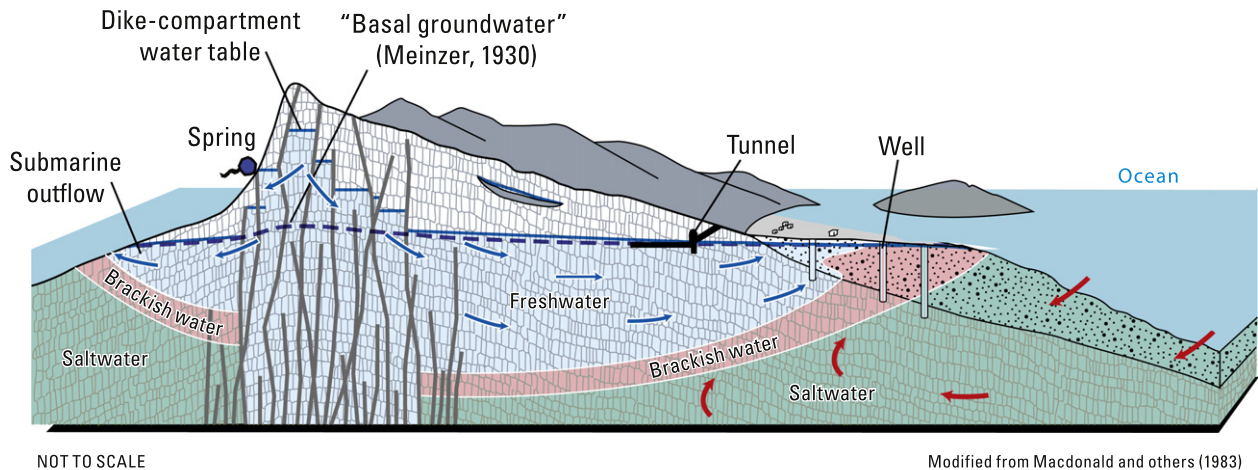


Fig. 1. Generalized conceptual model of a volcanic island showing dike-compartmentalized and basal groundwater tables.

1.2. Volcanic island heat flow

Thermal conductivity and basal heat flux likely affect water levels and temperatures in active volcanic island aquifer systems. Reported thermal conductivity is $0.5\text{--}4.5\text{ W m}^{-1}\text{ K}^{-1}$ for all high-porosity volcanic rocks including lava, tuffs, breccias, mid-ocean ridge basalts (Clauser and Huenges, 1995), with a narrower range of $1.5\text{--}2.5\text{ W m}^{-1}\text{ K}^{-1}$ for basalt (Deming, 2001). Water-saturated thermal conductivity values of 61 basalt samples from Hawaii ranged from $0.84\text{ W m}^{-1}\text{ K}^{-1}$ to $2.4\text{ W m}^{-1}\text{ K}^{-1}$ for bulk densities of $0.8\text{--}3.0\text{ g cm}^{-3}$ (Horai, 1991). A water-saturated thermal conductivity value of $1.75\text{ W m}^{-1}\text{ K}^{-1}$ was assigned to the basalt aquifer for thermal modeling of the Piton de la Fournaise volcano (Violette et al., 1997); an average value of $2.17\text{ W m}^{-1}\text{ K}^{-1}$ is estimated for basalts of the Lanzarote Volcano of the Canary Islands (Fernandez et al., 1992); values 2.5 and $2.0\text{ W m}^{-1}\text{ K}^{-1}$, respectively were used to represent the basal and upper volcanic units in coupled flow/thermal simulations of the Cascade Mountains (Hurwitz et al., 2003).

Background heat flux at volcanic islands is poorly known because of the lack of deep boreholes needed for conductive heat flow measurements and the perturbing effects of advective fluid flow. Basal heat flux likely depends on a combination of factors that include the age of the oceanic plate and presence or lack of magma bodies at depth, and the history and vigor of volcanism. Across the Cape Verde rise, oceanic heat flow measurements range between $0.045 \pm 0.003\text{ W m}^{-2}$ offswell to $0.064 \pm 0.004\text{ W m}^{-2}$ near the peak geoid anomaly (Courtney and White, 1986). This near-peak heat flow value is approximately 0.010 W m^{-2} higher than predicted by the conductive cooling model GDH1 (Stein and Stein, 1992) for the 125 Ma oceanic crust that Cape Verde sits on. Harris and McNutt (2007) reviewed heat flow data at four other oceanic hotspots (Hawaii, Reunion, Crozet, Bermuda) and found heat flow anomalies with magnitudes between 0.005 and 0.014 W m^{-2} relative to GDH1; based on large measurement variability and small heat-flow anomalies associated with these oceanic hotspots, they suggested that hydrothermal circulation may be redistributing the heat such that the full magnitude of sublithospheric thermal variations may not be imaged. Subsequently, Stein and Von Herzen (2007) came to the opposite conclusion that while hydrothermal circulation may locally redistribute heat, sublithospheric thermal anomalies do not mask a broad heat flow anomaly. This view is supported by wide-angle seismic data that images the flexure of the Cape Verde swell. These data yield an effective elastic thickness value of 30 km for 125 Ma oceanic lithosphere, leading Pim et al. (2008) to conclude that a broad thermal anomaly associated with the Cape Verde swell does not exist. Yet locally, basal heat flux in

active volcanic regions may be high. For example, at Hawaii the background heat flow anomaly is about 0.010 W m^{-2} above the expected heat flow of 0.058 W m^{-2} (Von Herzen et al. 1982; Harris et al. 2000); basal heat flux values up to about 0.8 W m^{-2} are reported from deep boreholes on the Kilauea volcano, with much lower values (up to 0.08 W m^{-2}) away from the volcano (Kauahikaua, 1993).

2. Site description

Cape Verde is located at approximately $16^\circ\text{N } 24^\circ\text{W}$ in the Atlantic Ocean off the west coast of Africa (Fig. 2). The islands are comprised of tholeiitic basalts formed by hot spot activity east of the Mid-Atlantic Ridge beneath the African plate (Barmen et al., 1990), a process similar to that by which the Hawaiian Islands were created (Natland, 1978). The easternmost islands formed ca. 10–20 Ma, whereas the western ones are generally younger than 8 Ma (Courtney and White, 1986; Christensen et al., 2001). Groundwater conditions were recently studied in watersheds on three of Cape Verde's islands: Mosteiros Basin on Fogo, Ribeira Paul on Santo Antão, and Ribeira Fajã on Sao Nicolau (Heilweil et al., 2006). The island of Fogo is the youngest and most active volcano in the Cape Verde Islands; its most recent eruption occurred in 1995 (Silva et al., 2004). Unlike the other islands, Fogo consists of a single volcano and, thus, is in the form of a nearly spherical cone about 25 km in diameter (area of 475 km^2), with the 2900 m main peak (tallest point in the Atlantic Ocean) at its apex. The summit caldera, known as Cha das Caldeiras, has a diameter of about 8 km. The relatively flat caldera floor is at an altitude of about 1600–1800 m, rimmed by near-vertical walls up to altitudes of about 2500 m. The island is comprised of eight surface watersheds draining radially from the caldera rim towards the ocean (Kallrén and Schreiber, 1988). Researchers have unsuccessfully attempted to locate the groundwater table in the upland areas of the Island of Fogo using surface geophysical methods, including Vertical Electrical Sounding (VES) and Electromagnetic Resistivity Profiling (VLF-r) along the flanks of the volcano (Kallrén and Schreiber, 1988) and Time Domain Electromagnetic (TDEM) surveys within the central caldera (Desclotres et al., 2000).

The Mosteiros Basin watershed covers an area of 42 km^2 on the northeastern side of the Island of Fogo (Fig. 3). The southern boundary of the surface watershed of the basin is the caldera rim. The watershed ranges in altitude from 0 to 2400 m, with an average elevation of 820 m (Table 1). Of the three watersheds previously studied (Heilweil et al., 2006), Mosteiros Basin was selected for applying coupled flow/thermal modeling for evaluating



Fig. 2. The Cape Verde Islands, West Africa.

volcanic island groundwater conditions for several reasons. The proximity of the Mosteiros Basin to the volcanically active caldera allows an investigation of the thermal affects associated with the interaction between warm upward conductive basal heat flux and cool downward advection associated with groundwater recharge. Also, unlike the other two watersheds, groundwater development along the coastal plain in Mosteiros Basin has caused salt-water intrusion; thus there is a greater need for understanding upland aquifer characteristics to guide future groundwater resources development. Furthermore, its relatively simple topography, consisting of a uniform volcanic slope without the deeply incised canyons present in the Ribeira Paul and Ribeira Fajã watersheds, is more amenable to representation with a simple two-dimensional spatial grid. Finally, evaluating the potential for upland groundwater development in watersheds of recently formed volcanic islands such as Mosteiros is more critical than in basins where the land surface of deeply incised drainages either approaches or intersects the water table, allowing for inland spring discharge and (or) groundwater accessible to shallow wells.

Because of the basin's steep topographic gradient and lack of deeply incised drainages (typical of recently formed volcanic

slopes), there are no large perennial upland springs; all measurable groundwater discharge from Mosteiros occurs as springflow and well production along the narrow coastal plain. This measurable groundwater discharge (not including submarine outflow) is about $600 \text{ m}^3 \text{ d}^{-1}$ and includes Monte Vermelho spring and production wells along the coast (Fig. 3). Monte Vermelho spring, with an estimated discharge of about $500 \text{ m}^3 \text{ d}^{-1}$, emanates at the coastline from the base of columnar basalts. Production wells FF 21 and FF 22 collectively pump an additional $100 \text{ m}^3 \text{ d}^{-1}$ (Água Brava L. da Delegação dos Mosteiros, personal communication, 2006). Substantial groundwater discharge from Mosteiros Basin as submarine outflow also likely occurs but has not been quantified; an ocean thermographic study by the Institut Géographique National de France (1981) located several springs off the northern coast of Fogo discharging fresh water below sea level.

2.1. Geology and hydraulic properties

The geology of the Mosteiros Basin has been previously described in detail by Kallrén and Schreiber (1988) and Barmen et al. (1990). The basin is dominated by basaltic lava flows with

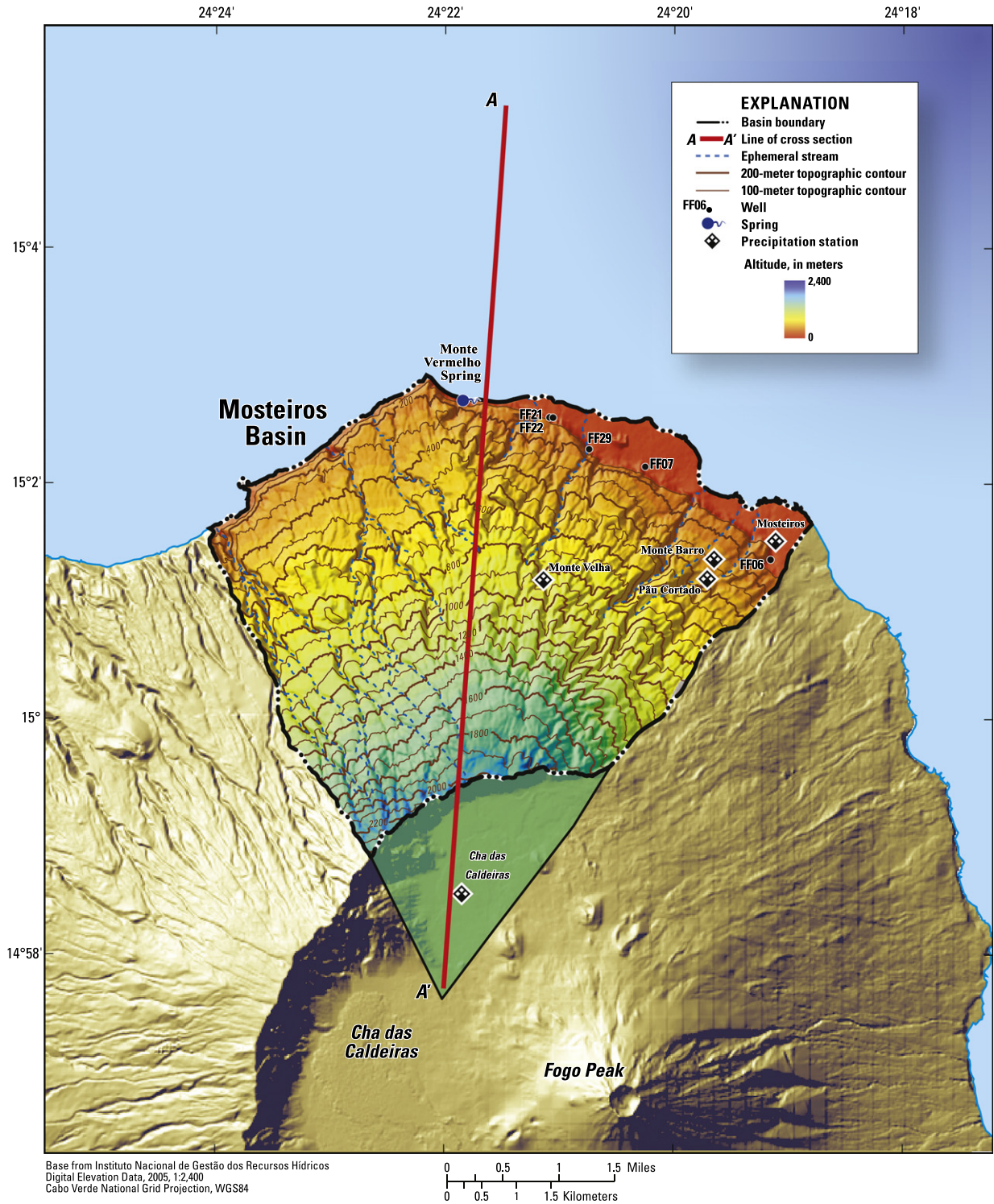


Fig. 3. Topography and hydrologic features of Mosteiros Basin and Cha das Caldeiras, Fogo Island.

intercalated pyroclastic deposits; the basin is also dotted with numerous cinder cones made of coarse volcanic fragments (Fig. 4). Older lava flows comprise the Basal Eruptive Complex (BEC) and, in places, have been highly altered to low permeability clays and have been intruded by a dense network of igneous dikes. Basaltic lava flows of the Principal Eruptive Complex (PEC) overlie the BEC. The PEC consists of lava flows that form fairly continuous steeply dipping layers (20–30°) from the island’s central caldera complex to the sea that may be important conduits of groundwater flow. Unlike the BEC, igneous cross-cutting dikes in the

PEC are sparse and only observed along the northern part of Mosteiros Basin near Monte Vermelho. Because of fracturing, both the BEC and PEC are considered to contain substantial permeability and, thus, act as components of the groundwater system. In contrast, fractures and pores in the volcanic rocks of the underlying Ancient Complex (CA) are well-cemented, resulting in low-permeability (clay-like) properties. The top of the CA, therefore, is assumed to be the lower boundary of the aquifer system. An east-west geologic cross section of Fogo indicates that the BEC/CA boundary occurs at an altitude slightly below sea level about

Table 1
Hydrologic characteristics for selected Cape Verde watersheds.

Watershed	Mosteiros	Paul	Fajã
Area (km ²)	42	15	16
Average topographic slope (°)	27	38	23
Maximum altitude (m)	2400	1500	1300
Average altitude (m)	820	620	480
Average annual precipitation (mm)	590	670	310
Total precipitation (m ³ d ⁻¹)	68,446	27,379	13,689
Measured groundwater discharge (m ³ d ⁻¹)	620	4030	450
Discharge as percent of precipitation	1	15	3

8 km southeast of Cha das Caldeiras. The depth of this boundary is consistent with low electrical resistivity VES measurements (100–250 Ω m) of Fogo (Kallrén and Schreiber, 1988).

There are no available hydraulic conductivity data for the basalts in Mosteiros Basin. Such information is available from the Ribeira Fajã watershed (Sao Nicolau); dewatering in the mid-1980s, associated with the construction of a water tunnel, yielded estimated transmissivity values of about 10⁻⁵–

10⁻⁴ m² s⁻¹ (Heilweil et al., 2006). Assuming an aquifer thickness of 100 m, estimated hydraulic conductivity (K_{sat}) values range from 10⁻⁷ to 10⁻⁶ m s⁻¹.

2.2. Temperature, precipitation, and infiltration

Mean annual air temperature at sea level in Cape Verde is about 25 °C (Langworthy and Finan, 1997). Air temperature decreases with altitude; a study on the island of Santiago indicates that mean annual air temperature is 22 °C at an altitude of about 400 m (Sabiño et al., 1999). Mean annual ground-surface temperature is generally considered to be within a few degrees of mean annual air temperature (Powell et al., 1988; Putnam and Chapman, 1996). For this study, a ground-surface temperature lapse rate was constructed based on the relation between altitude and measured water temperature for 64 springs throughout Cape Verde (Fig. 5). This assumes that discharging springs are in thermal equilibrium with mean annual ground-surface temperature. While this may not be the case for springs having large discharge rates, most of the springs shown in Fig. 5 have discharge rates of less than 100 m³/d. Spring temperatures and altitudes ranged from about

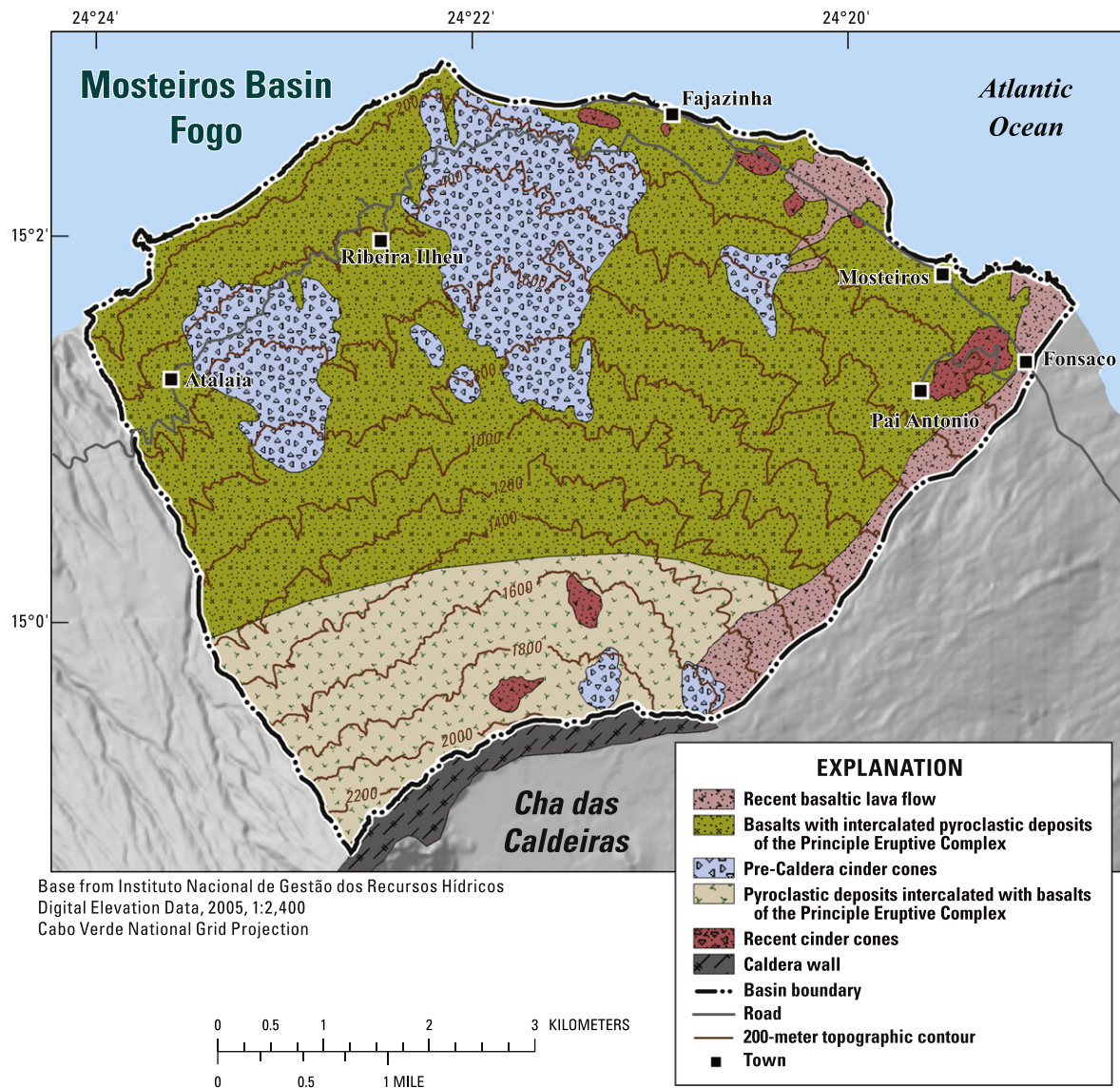


Fig. 4. Geology of Mosteiros Basin, Fogo Island.

12 to 26 °C and 0 to 2000 m, respectively. The observed inverse linear correlation between temperature and altitude of -7.5 °C per 1000 m ($r^2 = 0.78$) supports the assumption that the springs are in approximate thermal equilibrium with the land surface. A lapse band width of about 3 °C accounts for 2σ (95%) of the variation in measured temperatures at similar altitudes (Fig. 5).

The primary source of precipitation in the Mosteiros groundwater basin is Atlantic monsoonal moisture associated with the northward migration of the Inter-Tropical Convergence Zone (ITCZ), transported by the northeasterly trade winds (Kallrén and Schreiber, 1988; Sabino et al., 1999). An isohyetal map for Fogo based on 1945–1970 precipitation data (Vailloux and Bourguet, 1974) shows that precipitation rates are controlled by altitude and orientation with respect to these trade winds. Maximum precipitation rates for the island occur at mid-slope elevations in Mosteiros Basin on the northeastern side of the island; a rain shadow exists on the dry southwestern (leeward) side. A similar precipitation pattern is found on La Réunion in the Indian Ocean (Violette et al., 1997). The Vailloux and Bourguet (1974) precipitation map shows rainfall in Mosteiros Basin increasing about five-fold from the coastal plain near sea level to a maximum in the vicinity of the Monte Velha meteorology station (850-m altitude), then decreasing further inland towards the Cha das Caldeiras volcanic caldera (1600-m altitude; Fig. 3). While this previously published precipitation pattern was adopted for the current study, the absolute values were reduced by 50%, resulting in about 200 mm along the coastal plain, 800 mm at Monte Velha, and 400 mm in Cha das Caldeiras (Fig. 6). This reduced amount (see explanation in Fig. 6) is consistent with reported precipitation on Fogo varying between 200 and 1000 mm yr⁻¹ (Descloitres et al., 2000). The weighted-average precipitation along the 9-km transect of the Mosteiros groundwater basin shown in Fig. 6 is 550 mm yr⁻¹.

Because of the typically short-duration, high-intensity precipitation events and steep topography on Cape Verde, runoff intensities can exceed 100 mm h⁻¹ (Dittrich, 1982). This runoff has historically caused devastating flooding; stream discharge data from three watersheds having average topographic slopes of about 1–3° on the island of Santiago indicated that about 60% of average

annual rainfall was lost as runoff to the ocean (Sabino et al., 1999). The percent of runoff is likely higher in the Mosteiros Basin, having an average topographic slope of 27°. A lesser but significant portion of precipitation is consumptively used as evapotranspiration; annual potential evapotranspiration rates of up to 1300 mm have been reported for Cape Verde (Sabino et al., 1999).

Infiltration of the remaining moisture below the root zone is assumed to become groundwater recharge. Recharge to the Mosteiros groundwater basin is assumed to include both the Mosteiros watershed (42 km²) and a part (6.4 km²) of the closed Cha das Caldeiras basin, which has highly permeable surficial sediments and no surface-water outlet (Fig. 3). Recharge in Mosteiros basin is estimated using a previously published empirical relation between precipitation and recharge for the Cape Verde Islands: $R = 0.25(P - 300)$, where R is recharge and P is average precipitation, both in mm yr⁻¹ (Vailloux and Bourguet, 1974). Although this empirical relation is based on a period of above-average precipitation, the estimated recharge rates should scale down appropriately since a smaller percent of each watershed would receive greater than 300 mm annual precipitation during droughts ($R = 0$ for $P < 300$ mm). Dividing the cross-sectional precipitation pattern for Mosteiros Basin into two segments (less than and greater than 300 mm annual precipitation) and then applying this ratio yields a transect-averaged annual infiltration rate of about 70 mm (3 Mm³ yr⁻¹ for the groundwater basin), or about 12% of the average weighted precipitation rate of 550 mm yr⁻¹. Measured groundwater discharge from the basin was previously reported to be about 0.2 Mm³ yr⁻¹ (Heilweil et al., 2006), or only about 1% of total estimated precipitation. For comparison, groundwater discharge/precipitation ratios of 3% and 15% were derived for the Ribeira Fajã and Ribeira Paul basins, respectively (Heilweil et al., 2006). This indicates that most of the groundwater may be leaving the Mosteiros Basin as submarine groundwater discharge.

2.3. Water-table depth

Previous groundwater studies of Fogo have hypothesized the presence of relatively high-altitude regional water tables beneath

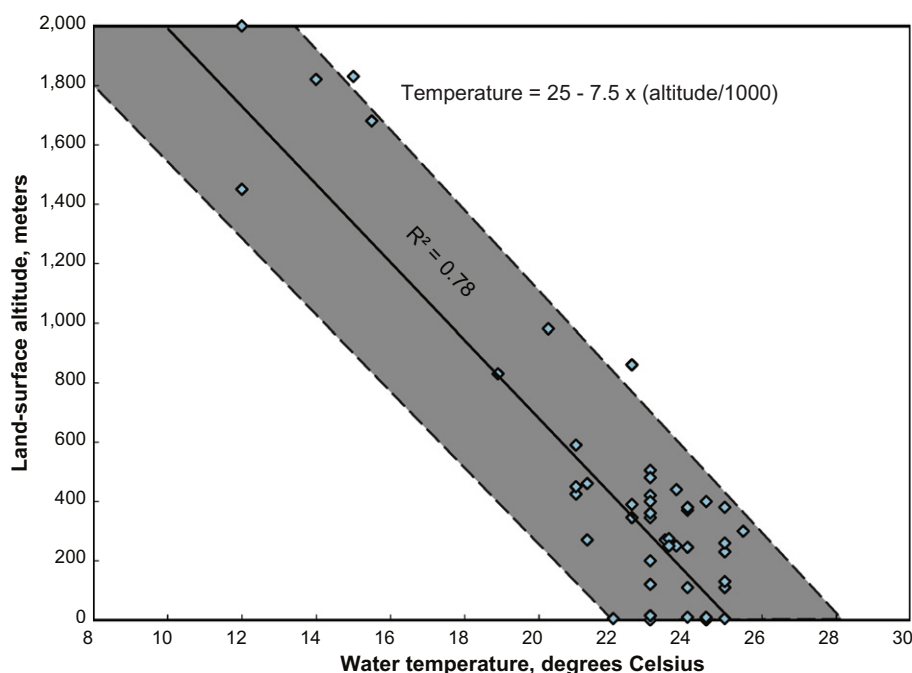
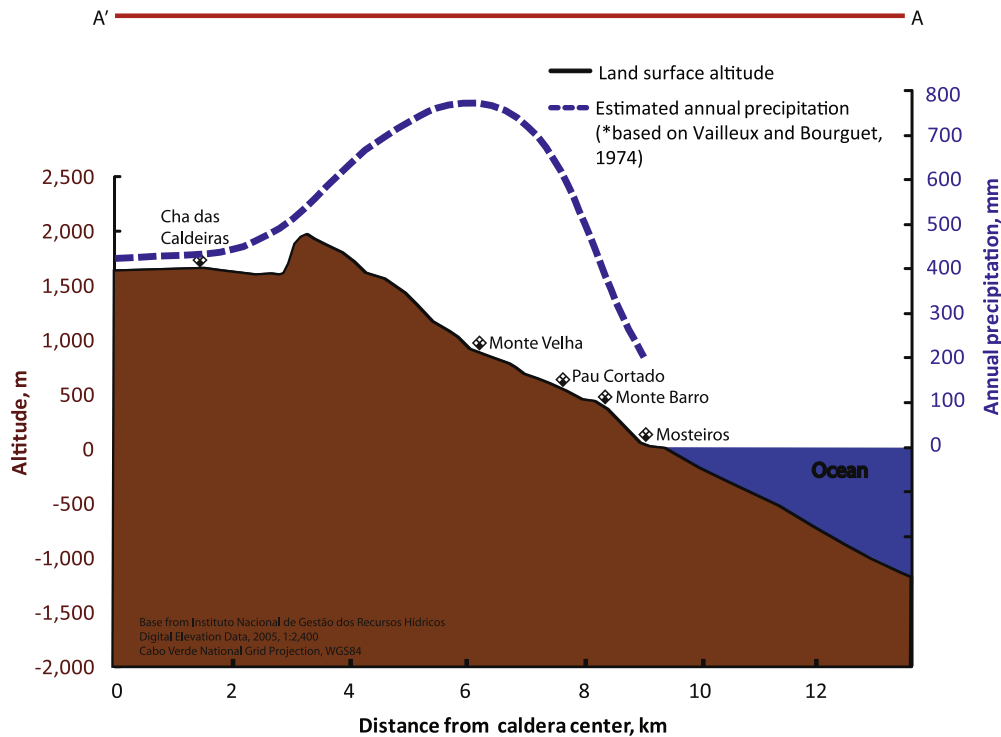


Fig. 5. Relation between altitude and water temperature for springs in Cape Verde.



*The published Vailloux and Bourguet (1974) precipitation values of 350 to 1,500 mm yr⁻¹, based on data from 1945–1970, are higher than other precipitation records and were reduced by 50 percent. This other data including three stations within the basin (Heilweil et al., 2006): 1996–2002 annual averages of 210 mm at Mosteiros Station (75-m altitude), 350 mm at Monte Barro Station (350-m altitude), and 380 mm at Pau Cortado Station (460-m altitude). Lower precipitation rates are also supported by longer-period records from elsewhere in Cape Verde, indicating that the 1945–1970 period was anomalously wet. These supporting precipitation records include 1945–1986 at the 1,150-m altitude Achada Fora station 10 km southwest of Mosteiros Basin (Kallrén and Schreiber, 1988), 1945–2005 at the 750-m altitude Cachaço station on the island of Sao Nicolau (Olivry, 1981; Sabino, 1986; Heilweil et al., 2006), and 1941–1996 at the 300-m altitude São Jorge station on the island of Santiago (Sabino et al., 1999).

Fig. 6. Altitude and estimated annual precipitation along the A–A' north–south transect (refer to Fig. 3 for location) of Mosteiros Basin.

the volcanic summits and calderas (Kallrén and Schreiber, 1988; Barmen et al., 1990; Heilweil et al., 2009). However, the steep topography, high drilling costs, and limited road access have precluded the drilling of deep exploratory wells in the upland parts of Fogo, so little is known about groundwater conditions in the interior of the volcanic edifice. Water-table information is limited to: (1) water level measurements from five wells at land surface altitudes of 20–60 m showing a water table altitude near sea level; (2) the Monte Vermelho Spring in Mosteiros Basin (Fig. 3; Heilweil et al., 2006) and altitudes of other large coastal springs elsewhere on Fogo (Kallrén and Schreiber, 1988); (3) a 200-m altitude water table, determined from a 100-m deep well at a land-surface altitude of 300 m on the northwest side of Fogo (Barmen et al., 1990); (4) a water-table altitude less than 320 m at a land-surface altitude of 500 m, determined from a 180-m deep dry borehole near the village of Patim in the southwest part of Fogo (Barmen et al., 1990); and (5) a water-table altitude less than 1200 m at a land-surface altitude of 1600 m in Cha das Caldeiras, determined from three dry geothermal research holes (INGRH, written commun., 2011) and TDEM surveys, which found no evidence of groundwater shallower than 400 m depth (Descloitres et al., 2000).

2.4. Environmental-tracer evidence of a deep vadose zone

Groundwater environmental tracer samples from Mosteiros Basin indicate a predominantly meteoric source of water (rather than magmatic fluids) and a mixture of groundwater residence times. Groundwater stable-isotope concentrations indicate a relatively high-altitude precipitation source. Samples collected in both 2005 (Heilweil et al. 2009) and 2009 (Table 2) have $\delta^{18}\text{O}$ values

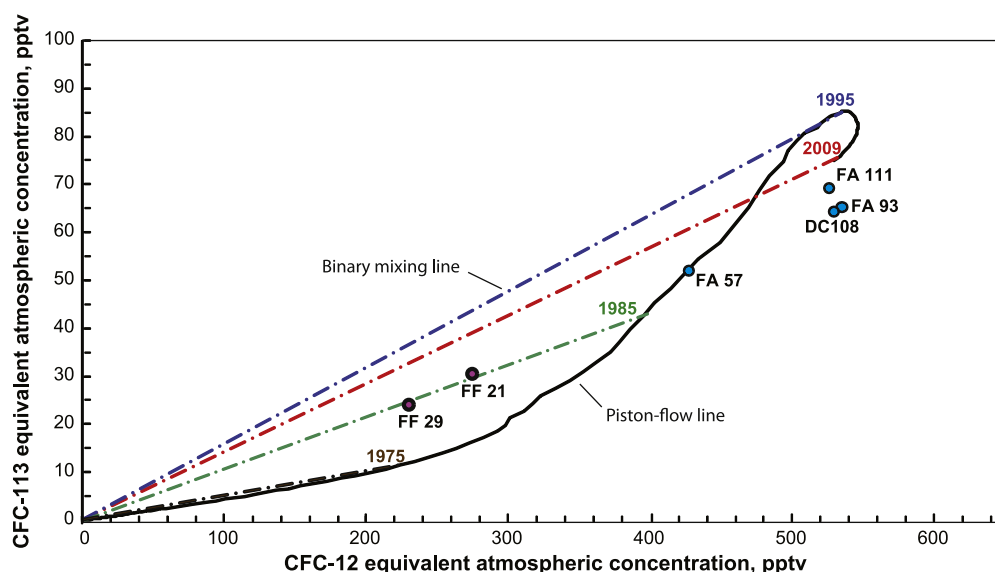
ranging from -5.1‰ to -3.4‰ . These values are on the more depleted end of the -0.5‰ to -4.8‰ range of previously published Cape Verde precipitation data (Barmen et al., 1990; Heilweil et al., 2009). Tritium concentrations range from 0.0 to 1.2 tritium units (TU), indicating a mix of pre-modern (prior to the 1950s) and modern groundwater. Chlorofluorocarbon (CFC) concentrations indicate that groundwater at two sites in Mosteiros Basin (FF 21, FF 29) are a binary mixture of recent and pre-modern recharge. This observation is illustrated in a plot of CFC-12 against CFC-113 concentration (Fig. 7). Based on multiple-tracer lumped parameter methods described by Böhlke (2006), FF 21 and FF 29 plot along the 1985 binary mixing line. Their positions on this line indicate a possible binary mixture of about 60% mid-1980s recharge with 40% pre-1950s recharge. Measured carbon-14 concentrations of 46–74 pmc are also consistent with a mixture of recent and pre-modern recharge. It is important to note that this binary mixing model is not unique, as there are an unlimited number of age mixtures that could produce these CFC concentrations.

A comparison of CFC-12 and tritium concentrations, however, shows that some samples, such as well FF 21 in Mosteiros Basin, fall below both the piston-flow and mid-1980s binary mixing lines. While the other samples plot along these lines, some sites have higher-than-expected CFC concentrations for their measured tritium concentrations (Fig. 8). This relationship is attributable to modern CFC-rich air arriving at the water table beneath a thick vadose zone faster than the downward migration of modern tritium-rich infiltration. This deep earlier arrival of CFCs is likely caused by barometric pumping of modern atmospheric gases. Such barometric pumping in the unsaturated zone of fractured rocks was first proposed by Nilson et al. (1991) and leads to discrepancies in

Table 2

Recent (2009) environmental tracers results of groundwater in the Mosteiros and Ribeira Paul Basins, Cape Verde.

Site name	FF 21	FF 29	DC 108	FA 57	FA 93	FA 111
Date	7/24/2009	7/24/2009	7/21/2009	7/21/2009	7/21/2009	7/21/2009
Sample type	Well	Well	Spring	Well	Well	Well
Basin	Mosteiros	Mosteiros	Paúl	Paúl	Paúl	Paúl
Latitude (DMS)	150246	150229	170816	170820	170849	170833
Longitude (DMS)	0242104	0242043	250240	0250140	0250104	250220
Altitude (m)	40	60	268	80	20	126
Specific conductance ($\mu\text{S}/\text{cm}$)	520	1170	350	560	650	652
pH (standard units)	7.6	7.5	8.4	7.8	7.7	8.3
Temperature ($^{\circ}\text{C}$)	23.4	25.5	24.2	24.4	23.6	26.4
$\delta^2\text{H}$ (permil)	-18.5	-18.2	-15.0	-14.08	-13.7	-16.0
$\delta^{18}\text{O}$ (permil)	-3.81	-3.88	-3.36	-3.09	-2.95	-3.15
^3H and precision (TU)	0.0 ± 0.1	0.5 ± 0.1	0.5 ± 0.1	0.8 ± 0.1	1.0 ± 0.1	1.0 ± 0.1
CFC-11, pptv	98	68	170	159	189	165
CFC-12, pptv	275	230	530	426	534	525
CFC-113, pptv	31	24	64	52	65	68
^{14}C , pmc	46.0	73.9	-	-	-	-
$\delta^{13}\text{C}$, permil VPDB	-7.31	-8.24	-	-	-	-



The black piston-flow line indicates the relation between CFC-12 and CFC-113 for water samples in equilibrium with atmospheric CFCs from the 1950s through 2010. The colored dashed lines represent binary mixes of pre- and post-1950s groundwater recharge. The intersection of the colored dashed lines with the piston-flow line indicates expected historical equivalent atmospheric CFC concentrations of water that equilibrated with air during 1975, 1985, 1995, and 2009.

Fig. 7. CFC-12 versus CFC-113 concentrations of groundwater from sites in Mosteiros and Ribeira Paul Basins, Cape Verde.

age-dating using gaseous tracers in deep (>10 m) water-table settings (Cook and Solomon, 1995). This mechanism has been invoked as the explanation for the presence of modern atmospheric CFC-12 concentrations at great depth (>50 m) in the unsaturated zone of basalts of the Snake River Plain (Plummer et al., 2000) and the High Plains Aquifer of Texas (Weeks et al., 1982). The arrival of modern atmospheric CFCs ahead of liquid-phase infiltration (containing tritium) provides additional qualitative evidence for a relatively thick vadose zone in the Mosteiros Basin recharge area. No such discrepancy is found at other sites (such as FF29), indicating shallower water-table depths in other parts of the basin.

3. Methods and theory

3.1. Noble-gas thermometry

Noble-gas thermometry was used to evaluate water-table temperature in the recharge zone of Mosteiros Basin and the other two studied watersheds. Our initial hypothesis was that the increased

basal heat flux and the geothermal gradient associated with volcanic activity would significantly warm groundwater temperatures in the upland portion of the aquifer along the flank of the active caldera. As recharge enters an aquifer, atmospherically derived noble gas concentrations are a function of temperature, salinity, atmospheric pressure, and excess air (Aeschbach-Hertig et al., 1999; Ballentine and Hall, 1999; Stute and Schlosser, 2001; Mazar and Verhagen, 1976). High $\text{N}_2/^{40}\text{Ar}$ ratios, low pH, and elevated P_{CO_2} (causing elevated total-dissolved gas pressure) have been previously associated with actively circulating geothermal fluids (Chiodini et al., 1995; Dallai et al., 2005; Wood, 2006). In Cape Verde, low $\text{N}_2/^{40}\text{Ar}$ ratios of less than 45, relatively neutral pH, and ambient total-dissolved gas pressures confirm that dissolved noble gases are primarily of atmospheric origin, rather than from mantle outgassing (Heilweil et al., 2009). Because atmospheric dissolved gases are relatively inert and there is no evidence of in situ gas production or gas stripping in collected noble-gas samples, it is assumed these gases remain relatively unchanged during groundwater transit to well and spring sampling sites.

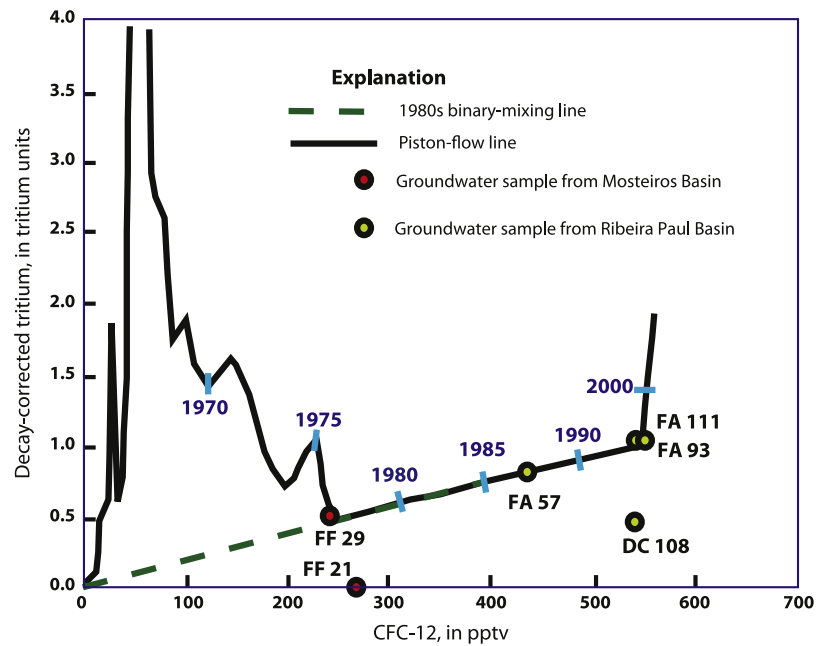


Fig. 8. CFC-12 versus tritium concentrations of groundwater from sites in Mosteiros and Ribeira Paul Basins, Cape Verde.

Noble-gas samples were collected as water samples in copper tubes (Weiss, 1968; Stute and Schlosser, 2001) and as gas samples with in situ diffusion samplers (Sheldon, 2002). Noble-gas concentrations of ^{20}Ne , ^{40}Ar , ^{84}Kr , and ^{129}Xe were analyzed by the University of Utah's Dissolved Gas Service Center using isotope dilution with Stanford Research Instruments RGA300 quadrupole mass spectrometers. For samples collected in copper tubes, gas was stripped and collected under vacuum for inlet to the mass spectrometer to determine noble-gas concentrations. Gas samples from diffusion samplers were inlet directly to a mass-spectrometer for determination of relative mole fractions, which were converted to concentrations using field measurements of total dissolved-gas pressure and water temperature. Analytical precision was estimated to be 2% for ^{20}Ne , 3% for ^{40}Ar , 4% for ^{84}Kr , 5% for ^{129}Xe (Solomon, written commun., 2011). Recharge parameters were derived from the measured noble-gas concentrations assuming the closed equilibration (CE) model of excess air formation (Aeschbach-Hertig et al., 2000). Derived recharge parameters include: recharge temperature (T_r), the temperature at the water table at the point of recharge; the amount of initially trapped air per unit mass of water (A_e); and fractionation (F), which reflects the degree of subsequent dissolution of these trapped air bubbles. Recharge parameters were computed using a chi-squared (χ^2) minimization code (an Excel spreadsheet program with the built-in "Solver" inversion routine) like that described by Aeschbach-Hertig et al. (1999) and Manning and Solomon (2003). A χ^2 probability threshold ($P < 5\%$) of 3.8 (based on four measured gases and three recharge parameters) was used to define an acceptable fit for T_r , A_e , and F.

A recharge altitude must be assumed in order to derive a recharge temperature from noble-gas concentrations. A range of possible recharge temperature/altitude combinations were derived for each groundwater sample. The maximum recharge temperature ($T_{r_{\max}}$) was computed assuming a recharge altitude equal to the land-surface altitude at the sample location (the minimum altitude where recharge could occur). The minimum recharge temperature ($T_{r_{\min}}$) was computed assuming a recharge altitude equal to the highest possible water-table altitude within the watershed. The resulting range of possible recharge temperatures and altitudes for the sample is indicated by a line connecting the $T_{r_{\max}}$ and $T_{r_{\min}}$

points on a plot of recharge temperature versus altitude (" $T_{r_{\min}}/T_{r_{\max}}$ line"). Following the approach described by Manning and Solomon (2003), this range can be further constrained (reduced) by the intersection of the $T_{r_{\max}}/T_{r_{\min}}$ line with a local water-table temperature lapse band.

3.2. Coupled groundwater flow and heat transport

A two-dimensional numerical model of coupled groundwater flow and heat transport was developed to represent radial unconfined groundwater flow and heat transport from the interior of an active volcanic island towards the coast. The model was used to evaluate the influence of basal heat flux, recharge rate, and hydraulic and thermal properties on inland water-table altitude and temperature. Although the numerical model was specifically designed and calibrated to groundwater and temperature conditions for Mosteiros Basin on the island of Fogo, simulation results have the potential to be generalized to other active volcanic island settings due to the general lithologic and morphologic similarity of basaltic shield volcanoes.

Simulations were conducted using the VS2DH modeling software (Healy and Ronan, 1996; Hsieh et al., 1999). VS2DH uses the finite difference method to solve the Richards equation and the energy transport equation. The Richards equation describes both saturated and partially saturated groundwater flow; the energy transport equation simulates the change in thermal storage as a function of thermal conduction, dispersion, convection, and heat sources/sinks. The two equations are coupled through the calculation of change in hydraulic conductivity as a function of temperature, thermal storage as a function of moisture content, heat convection as a function of groundwater velocity, and the heat source/sink term as a function of fluid sources and sinks. VS2DH assumes single-phase liquid water movement with constant and uniform water density and isotropic thermal conductivity. By simulating both partially and fully saturated conditions, the model allows for the water-table altitude to be a dependent parameter rather than a specified boundary condition. Further details of VS2DH are presented by Healy and Ronan (1996).

3.2.1. Simulation assumptions and simplifications

Because of sparse geologic, hydrologic, thermal, and climate data for Mosteiros Basin, exact replication of the aquifer system was neither practical nor possible. Instead, the goal of coupled groundwater flow and heat transport modeling was to identify a range in values of recharge and hydraulic conductivity for which simulated groundwater flow and temperature patterns were consistent with measured groundwater levels and temperatures, as well as recharge temperatures estimated from noble gas concentrations. Several simplifying assumptions are invoked in the modeling effort. The groundwater system was assumed to extend to a depth of 1 km below sea level where a no-flow boundary condition is assigned (see Section 2.1). Following the approach of Violette et al. (1997), groundwater is assumed to have a constant density; hence, movement of sea water into the groundwater system is not considered. Steady-state groundwater flow and heat transport within the aquifer system are assumed. Also, while groundwater cooling through lateral ocean-water circulation is a possibility, flow rates of seawater intrusion are likely small in Cape Verde because of relatively low hydraulic conductivity of both the basalts and poorly sorted debris flows generally found along the submarine flanks of volcanic islands. Therefore, a cooling term to account for this potential seawater intrusion was not included in the numerical simulations.

VS2DH simulates single-phase liquid water flow. Subsurface temperatures close to the magma chamber beneath Fogo may be sufficient to create multiphase (liquid/steam) conditions; however, simulated temperature and head were continuously monitored at all model grid cells, conditions were never conducive to steam formation in the simulations used for this analysis. In addition, no hot-spring or fumarole activity has been observed or previously reported in the watershed. It is recognized, however, that hydraulic conductivity changes with temperature because of the temperature dependence of viscosity of water. As temperature increases, the magnitude of hydraulic conductivity increases. For ease of comparison with other references, we let K_{sat} represent hydraulic conductivity at ambient temperature, which if unstated, is 20 °C.

Hydraulic conductivity is assumed to be isotropic within both the Principal Eruptive Complex (PEC) and the Basal Eruptive Complex (BEC). Although hydraulic properties may vary greatly in shield volcano basalts because of flow layering, fractures, and low-permeability dikes, these features have not been mapped in Mosteiros Basin, nor have their hydraulic properties been specifically evaluated. A

simplifying assumption of porous media flow, therefore, is invoked for all simulations. The uniform hydraulic conductivity values used in the model instead represent an averaging at the regional scale of localized aquifer heterogeneity and anisotropy.

3.2.2. Model configuration and boundary conditions

The model simulates groundwater flow and heat transport along a radial cross-section through a 9-km long transect from the central volcanic caldera to the ocean (Fig. 6). The top boundary of the model representing land surface (0–2 km altitude) is a specified flux and temperature boundary that simulates the net infiltration of precipitation (Fig. 9). The model bottom, at 1 km below sea level, is a groundwater no-flow boundary with specified basal heat flux. The vertical boundary at the southern side of the model beneath the caldera is simulated as a no-flow boundary; the vertical boundary at the northern side represents the coastline and is simulated as a specified-head boundary, where groundwater discharges at and below sea level. The two geologic units represented within the model are the PEC and BEC, located above and

Table 3
Constant hydrologic and thermal simulation parameters.

Parameter	BEC ^a value	PEC ^b value
Specific storage	0.00005 m ⁻¹	0.00005 m ⁻¹
Residual moisture content	0.04	0.02
van Genuchten alpha	1.00	4.31
van Genuchten n	1.23	3.1
Porosity	0.05	0.1
Thermal conductivity	2.2 W m ⁻¹ °C ⁻¹	2.2 W m ⁻¹ °C ⁻¹
Heat capacity of solids	2.18 × 10 ⁶ J m ⁻³ °C ⁻¹	2.18 × 10 ⁶ J m ⁻³ °C ⁻¹
Heat capacity of water	4.18 × 10 ⁶ J m ⁻³ °C ⁻¹	4.18 × 10 ⁶ J m ⁻³ °C ⁻¹
Basalt density	2500 kg m ⁻³	2500 kg m ⁻³
Infiltration temperature	10–25 °C	
Precipitation ^c	200–800 mm yr ⁻¹	

^a BEC, Basal Eruptive Complex.

^b PEC, Principal Eruptive Complex.

^c Spatial distribution shown in Fig. 6.

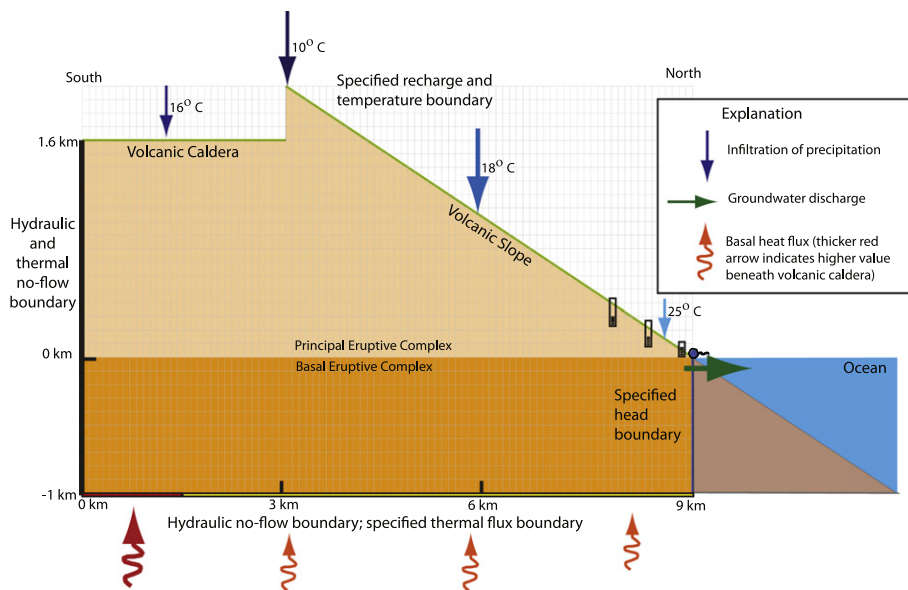


Fig. 9. Cross-sectional flow/heat transport model and boundary conditions along the A–A' north–south transect of Mosteiros Basin.

below sea level, respectively. Steady-state flow was assumed for all simulations. The domain was represented by a finite difference grid of cells with uniform height and width of 100 m.

Recharge was applied as a uniform percent of estimated annual precipitation (Table 3) and distributed spatially according to the profile shown in Fig. 6. Acknowledging the uncertainty in the recharge rate of 12% of precipitation derived from the Vailloux and Bourguet (1974) empirical relation, recharge was varied between 5% and 30% during model sensitivity analysis, resulting in weighted mean annual net infiltration ranging from about 30 mm to 170 mm. The temperature of infiltrating water is specified based on a temperature lapse rate of $-7.5\text{ }^\circ\text{C km}^{-1}$ and decreases linearly with altitude from about $25\text{ }^\circ\text{C}$ at sea level to $10\text{ }^\circ\text{C}$ at an altitude of 2 km (Fig. 5).

4. Results

4.1. Noble-gas recharge temperatures

Chi-square values were below the probability threshold ($p < 0.05$) of 3.8 for all but one sample (Table 4). This indicates acceptable recharge parameter model fits, consistent with a predominantly atmospheric origin of noble gases in these aquifers. Small amounts of excess neon (ΔNe typically $<10\%$) indicate little excess air in most samples. Relatively high dissolved-oxygen concentrations (3.0–7.9 mg/L) further support a predominantly atmospheric source of these noble gases. Only one sample (Well FA 57 in Ribeira Paul Basin) had an unacceptably high χ^2 value (23.7), and noble-gas recharge temperatures (NGTs) were not calculated for this site. It is possible that gas bubbles formed in the copper tube during sample collection, compromising sample integrity.

Calculated NGTs in the three Cape Verde watersheds are relatively cool, ranging from a Tr_{min} of about $11\text{ }^\circ\text{C}$ to a Tr_{max} of $22\text{ }^\circ\text{C}$ in Mosteiros Basin and from $15\text{--}24\text{ }^\circ\text{C}$ and $15\text{--}26\text{ }^\circ\text{C}$ in the Ribeira Paul and Ribeira Fajã Basins, respectively. Using a Monte Carlo approach described by Manning and Solomon (2003), a 1σ uncertainty in noble-gas recharge temperatures about of $\pm 2\text{ }^\circ\text{C}$ was computed for the NGTs derived for the Cape Verde samples using the CE model. As explained in Section 3.1, the Tr_{min} values are based on the highest possible water-table altitude in each basin (1900 m in Mosteiros, 1400 m in Ribeira Paul, 1200 m in Ribeira Fajã). Tr_{max} is based on the lowest potential altitude in the basin (sampling altitude). These NGTs are similar to measured spring temperatures throughout Cape Verde ($12\text{--}26\text{ }^\circ\text{C}$), suggesting that even on the flanks of the active Fogo volcano, water-table temperatures in the recharge zone of the aquifer system do not appear to be strongly influenced by the anomalously high heat flow.

4.2. Simulations of coupled groundwater flow and heat transport

The primary numerical modeling effort consisted of running a series of simulations over a wide range of recharge rates and hydraulic conductivities including vertical anisotropy (Series 1; Table 5); other model parameters were held constant for these simulations (Table 3). Other simulations (Series 2–6) were used to evaluate the sensitivity of other parameters including basal heat flux, thermal conductivity, thickness of the BEC, and porosity. We evaluated each simulation by comparing model output with observed groundwater levels, along with measured temperatures and NGT-derived recharge temperatures. A simulation was determined to be acceptable if four criteria were satisfied: (1) the water-table altitude at a distance of 8 km from the left-hand-side of the simulated domain (Fig. 9) was in the range of 150–250 m, (2) water-table temperature at that same location was $21.5\text{--}23.5\text{ }^\circ\text{C}$ based on measured groundwater temperatures in Mosteiros Basin (Table 4), (3) water-table altitude beneath the caldera (0 km from left-hand side) was less

Table 4 Selected field measurements, noble-gas concentrations, and estimated recharge temperatures of groundwater in the Mosteiros, Ribeira Paul, and Ribeira Fajã Basins, Cape Verde.

Name	Date	Altitude (m)	Total dissolved gas pressure (mm Hg)	Dissolved oxygen (mg/L)	Temperature ($^\circ\text{C}$)	^{40}Ar ($\text{cm}^3\text{ STP/g}$)	^{84}Kr ($\text{cm}^3\text{ STP/g}$)	^{20}Ne ($\text{cm}^3\text{ STP/g}$)	^{129}Xe ($\text{cm}^3\text{ STP/g}$)	ΔNe (%)	χ^2	F	A_e	Tr_{min} ($^\circ\text{C}$)	Tr_{max} ($^\circ\text{C}$)
Mt. Vermelho ^b	12/2/2005	5	763	7.6	22.2	3.0E-04	3.8E-08	1.7E-07	2.4E-09	3.7	0.1	0.00	0.000	15.3	22.3
FF 07 ^c	12/2/2005	20	747	7.5	22.8	3.2E-04	4.0E-08	1.8E-07	2.5E-09	9.6	0.0	0.90	0.071	15.5	22.1
FF 21 ^c	8/11/2005	40	766	7.1	23.0	3.1E-04	3.8E-08	1.7E-07	2.3E-09	2.7	0.3	0.97	0.126	19.0	22.3
FF 22 ^c	12/3/2005	40	756	7.1	22.4	3.3E-04	4.4E-08	2.2E-07	2.7E-09	3.1	2.6	0.00	0.003	11.4	19.3
FF 29 ^c	12/3/2005	60	758	6.4	22.7	3.7E-04	4.7E-08	1.9E-07	2.9E-09	13.0	0.2	0.87	0.140	12.6	16.7
Diaguito 1 ^d	12/8/2005	270	721	3.0	23.4	3.4E-04	4.1E-08	1.9E-07	2.6E-09	16.8	0.2	0.83	0.033	15.4	19.0
NA 21 ^d	8/6/2005	440	729	4.6	23.7	3.0E-04	3.8E-08	1.6E-07	2.2E-09	4.9	1.6	0.94	0.949	20.9	22.5
Passagem ^d	8/4/2005	300	730	5.7	22.6	3.0E-04	3.6E-08	1.7E-07	2.2E-09	5.4	0.3	0.94	0.109	21.7	23.9
Seladinha ^d	12/8/2005	460	712	6.5	21.3	2.9E-04	3.5E-08	1.6E-07	2.1E-09	1.8	0.6	0.98	0.122	21.6	23.3
Tabulera ^d	8/4/2005	840	689	7.5	18.9	3.0E-04	3.9E-08	1.6E-07	2.4E-09	1.7	0.2	0.98	0.179	17.1	17.8
FA 57 ^e	12/7/2005	80	777	5.0	24.0	3.2E-04	4.3E-08	3.4E-07	2.6E-09	5.3	23.7	0.00	0.008	– ^f	– ^f
FA 93 ^e	8/5/2005	20	745	5.3	23.0	3.3E-04	3.9E-08	1.8E-07	2.4E-09	11.5	1.0	0.88	0.117	20.6	23.4
Galleria Fajã ^g	8/18/2005	270	737	7.2	21.3	3.2E-04	3.9E-08	1.7E-07	2.6E-09	5.6	0.6	0.55	0.001	15.1	18.3
Galleria Fajã ^g	12/14/2005	270	744	7.9	21.3	3.1E-04	3.7E-08	1.5E-07	2.5E-09	–5.0	0.8	0.00	0.000	16.5	19.8
FN 39 ^h	12/13/2005	90	760	5.7	23.9	2.9E-04	3.7E-08	1.7E-07	2.1E-09	6.2	1.6	0.93	0.140	24	26.1

^a Tr_{min} is based on maximum possible water-table altitudes of 1900 m for Mosteiros, 1400 m for Paul, and 1200 m for Fajã.

^b Spring in Mosteiros Basin.

^c Well in Mosteiros Basin.

^d Spring in Ribeira Paul Basin.

^e Well in Ribeira Paul Basin.

^f Noble-gas recharge temperatures not calculated because of large χ^2 error.

^g Spring in Ribeira Fajã Basin.

^h Well in Ribeira Fajã Basin.

Table 5
Specified hydraulic and thermal properties, along with computed water-table altitudes and temperatures, for selected simulations.

Run	PEC and BEC thermal conductivity ($\text{W m}^{-1} \text{K}^{-1}$)	PEC K_{sat} (m s^{-1})	BEC K_{sat} (m s^{-1})	Recharge as fraction of precipitation	Inner caldera basal heat flux (W m^{-2})	Volcanic slope basal heat flux (W m^{-2})	PEC/BEC porosity	Water-table altitude at 0 km (m ASL)	Water-table altitude at 6 km (m ASL)	Water-table altitude at 8 km (m ASL)	Water-table temperature at 0 km ($^{\circ}\text{C}$)	Water-table temperature at 6 km ($^{\circ}\text{C}$)	Water-table temperature at 8 km ($^{\circ}\text{C}$)	Comments
<i>Series 1: Varying K_{sat} and recharge</i>														
1	2.2	1.00E-08	1.00E-08	0.120	0.1	0.1	0.10, 0.05	1550	917	250	13.2	18	23.4	Too high ^d
2	2.2	2.00E-08	2.00E-08	0.050	0.1	0.1	0.10, 0.05	543	359	136	20.6	22.8	26.1	Too warm ^b , too low ^c
3	2.2	2.00E-08	2.00E-08	0.085	0.1	0.1	0.10, 0.05	936	618	228	14.7	18.9	23.6	Too warm ^b , too low ^c
4	2.2	2.50E-08	2.50E-08	0.070	0.1	0.1	0.10, 0.05	643	417	162	17	20.6	24.8	Too warm ^b
5	2.2	2.50E-08	2.50E-08	0.100	0.1	0.1	0.10, 0.05	912	602	213	14.4	18.6	23.6	Too warm ^b
6	2.2	2.50E-08	2.50E-08	0.110	0.1	0.1	0.10, 0.05	997	668	250	14	18.3	23.4	Too high ^d
7	2.2	3.75E-08	3.75E-08	0.095	0.1	0.1	0.10, 0.05	629	404	160	15.5	19.5	24	Too warm ^b
8	2.2	3.75E-08	3.75E-08	0.120	0.1	0.1	0.10, 0.05	793	515	194	14.2	18.5	23.6	Too warm ^b
9	2.2	3.75E-08	3.75E-08	0.150	0.1	0.1	0.10, 0.05	971	652	231	13.6	17.9	23.4	Satisfies constraints ^e
10	2.2	3.75E-08	3.75E-08	0.190	0.1	0.1	0.10, 0.05	1173	774	250	13.3	17.7	23.4	Too high ^d
11	2.2	5.00E-08	5.00E-08	0.095	0.1	0.1	0.10, 0.05	496	314	117	16.1	19.9	24.5	Too warm ^b , too low ^c
12	2.2	5.00E-08	5.00E-08	0.120	0.1	0.1	0.10, 0.05	627	401	159	14.6	18.8	23.7	Too warm ^b
13	2.2	5.00E-08	5.00E-08	0.190	0.1	0.1	0.10, 0.05	960	625	228	13.4	17.7	23.3	Satisfies constraints ^d
14	2.2	5.00E-08	5.00E-08	0.210	0.1	0.1	0.10, 0.05	1036	683	250	13.3	17.7	23.4	Too high ^d
15	2.2	6.25E-08	6.25E-08	0.050	0.1	0.1	0.10, 0.05	196	121	46	24.6	25.5	27.9	Too warm ^b , too low ^c
16	2.2	6.25E-08	6.25E-08	0.095	0.1	0.1	0.10, 0.05	406	258	94	16.9	20.5	26.5	Too warm ^b , too low ^c
17	2.2	6.25E-08	6.25E-08	0.140	0.1	0.1	0.10, 0.05	606	387	153	14.3	18.5	23.4	Satisfies constraints ^e
18	2.2	6.25E-08	6.25E-08	0.190	0.1	0.1	0.10, 0.05	810	526	199	13.5	17.5	22	Satisfies constraints ^e
19	2.2	6.25E-08	6.25E-08	0.220	0.1	0.1	0.10, 0.05	915	596	219	13.3	17.6	23.2	Satisfies constraints ^e
20	2.2	6.25E-08	6.25E-08	0.250	0.1	0.1	0.10, 0.05	1013	670	250	13.3	17.6	23.4	Too high ^d
21	2.2	7.50E-08	7.50E-08	0.140	0.1	0.1	0.10, 0.05	521	329	122	14.4	18.7	23.2	Too low ^c
22	2.2	7.50E-08	7.50E-08	0.250	0.1	0.1	0.10, 0.05	887	579	212	13.3	17.6	23.1	Satisfies constraints ^e
23	2.2	7.50E-08	7.50E-08	0.300	0.1	0.1	0.10, 0.05	1037	684	250	13.2	17	20.3	Too high ^f , too cool
24	2.2	8.75E-08	8.75E-08	0.190	0.1	0.1	0.10, 0.05	614	399	154	13.7	18	22.9	Satisfies constraints ^e
25	2.2	8.75E-08	8.75E-08	0.250	0.1	0.1	0.10, 0.05	889	507	190	13.3	17.6	22.8	Satisfies constraints ^e
26	2.2	1.00E-07	1.00E-08	0.120	0.1	0.1	0.10, 0.05	783	557	236	15.8	19.4	23.4	Satisfies constraints ^e
27	2.2	1.00E-07	1.00E-07	0.120	0.1	0.1	0.10, 0.05	348	215	80	15.5	19.6	24.1	Too warm ^b , too low ^c
28	2.2	1.00E-07	1.00E-07	0.210	0.1	0.1	0.10, 0.05	608	387	154	13.6	17.6	21.7	Satisfies constraints ^e
29	2.2	1.00E-07	1.00E-07	0.250	0.1	0.1	0.10, 0.05	708	460	173	13.4	17.6	22.6	Satisfies constraints ^e
30	2.2	1.00E-07	1.00E-07	0.300	0.1	0.1	0.10, 0.05	840	558	205	13.3	17.1	20.8	Too cool ^a
31	2.2	1.20E-07	1.20E-07	0.250	0.1	0.1	0.10, 0.05	615	391	156	13.4	17.3	21.2	Too cool ^a
<i>Series 2: Varying basal heat flux</i>														
32	2.2	1.00E-08	1.00E-08	0.120	0.2	0.2	0.10, 0.05	1550	911	250	13.2	18.1	23.4	Too high ^d
33	2.2	1.00E-08	1.00E-08	0.120	1.0	0.1	0.10, 0.05	1416	910	250	13.9	18.3	23.4	Too high ^d
34	2.2	3.75E-08	3.75E-08	0.120	0.2	0.2	0.10, 0.05	688	456	173	15.5	20.1	25.2	Too warm ^b

(continued on next page)

Table 5 (continued)

Run	PEC and BEC thermal conductivity ($W m^{-1} K^{-1}$)	PEC K_{sat} ($m s^{-1}$)	BEC K_{sat} ($m s^{-1}$)	Recharge as fraction of precipitation	Inner caldera basal heat flux ($W m^{-2}$)	Volcanic slope basal heat flux ($W m^{-2}$)	PEC/BEC porosity	Water-table altitude at 0 km (m ASL)	Water-table altitude at 6 km (m ASL)	Water-table altitude at 8 km (m ASL)	Water-table temperature at 0 km ($^{\circ}C$)	Water-table temperature at 6 km ($^{\circ}C$)	Water-table temperature at 8 km ($^{\circ}C$)	Comments
35	2.2	3.75E-08	3.75E-08	0.120	1	0.1	0.10, 0.05	568	420	172	24.8	23.1	25.9	Too warm ^b
36	2.2	1.00E-07	1.00E-07	0.120	0.04	0.04	0.10, 0.05	390	241	89	14.1	17.8	22.2	Too low ^c
37	2.2	1.00E-07	1.00E-07	0.120	0.2	0.2	0.10, 0.05	294	183	69	18	22.6	27.4	Too warm ^b , too low ^c
38	2.2	1.00E-07	1.00E-07	0.250	0.2	0.2	0.10, 0.05	655	416	160	13.6	18.3	23.6	Too warm ^b
Series 3: Varying thermal conductivity														
39	1	2.00E-08	2.00E-08	0.085	0.1	0.1	0.10, 0.05	936	613	225	13.7	18.4	23.6	Too warm ^b
40	1	1.00E-07	1.00E-07	0.120	0.1	0.1	0.10, 0.05	350	215	80	14.1	19.1	24.1	Too warm ^b , too low ^c
41	1	1.00E-07	1.00E-07	0.250	0.1	0.1	0.10, 0.05	709	461	173	13.2	17.5	22.5	Satisfies constraints ^e
Series 4: Increasing BEC thickness to 1500 m														
42	2.2	5.00E-08	5.00E-08	0.120	0.1	0.1	0.10, 0.05	468	294	99	14	18.2	23.3	Too low ^c
Series 5: Varying porosity														
43	2.2	5.00E-08	5.00E-08	0.120	0.1	0.1	0.3, 0.3	639	403	159	14.6	18.8	23.7	Too warm ^b
44	2.2	5.00E-08	5.00E-08	0.210	0.1	0.1	0.3, 0.3	987	661	250	16.7	20.2	24.7	Too warm ^b , too low ^c
Series 6: Conductive heat transport (no recharge)														
45	2.2	1.00E-07	1.00E-07	0.000	0.1	0.1	0.10, 0.05	0	0	0	80.6	56.9	36	Too warm ^b , too low ^c

^a Water-table temperature at $x = 8$ km < 21.5 °C.

^b Water-table temperature at $x = 8$ km > 23.5 °C.

^c Water-table altitude at $x = 8$ km < 150 m.

^d Water-table altitude at $x = 8$ km > 250 m.

^e Satisfies water-table altitude and temperature constraints.

than 1200 m, and (4) water-table temperatures in the upland part of the aquifer (between 0 and 6 km from the left-hand side) were in the range of 11–22 °C, based on noble-gas temperatures.

Model results are most sensitive to values of hydraulic conductivity (K_{sat}) and recharge (R), as can be seen by simulated water-table altitudes and temperatures. Increasing the simulated recharge rate generally increases water-table altitudes and decreases groundwater temperatures. Increasing hydraulic conductivity, on the other hand, tends to lower water-table altitudes and increase water-table temperatures. The caldera location ($X = 0$ km) is subsequently used for the following comparisons because it shows the most response to changing model parameters. With K_{sat} of 10^{-8} m s⁻¹, R of 12% of annual precipitation (P), and basal heat flux (Q_h) of 0.1 W m⁻², the predicted water-table altitude is 1550 m (50 m below land surface) and yields a water table temperature of 13.2 °C (Run 1; Table 5). Increasing K_{sat} by an order of magnitude to 10^{-7} m s⁻¹ while leaving other parameter values unchanged (Run 27) results in a much lower altitude and warmer water table of 348 m and 15.5 °C (change in water-table altitude, $\Delta h = -1202$ m, and change in water-table temperature, $\Delta T = 2.3$ °C), respectively. With K_{sat} of 5×10^{-8} m s⁻¹ and R of 12% of P , increasing simulated transmissivity by increasing the BEC thickness from 1000 m (Run 12) to 1500 m (Run 42) also results in a lower-altitude but slightly cooler water table ($\Delta h = -159$ m, $\Delta T = -0.6$ °C).

Reducing recharge generally yields lower water-table altitudes and warmer water-table temperatures. For a K_{sat} of 6.25×10^{-8} m s⁻¹, decreasing recharge from 25% of P (Run 20) to 14% of P (Run 17) resulted in a decline in water-table altitude beneath the caldera and an increase in temperature ($\Delta h = -407$ m, $\Delta T = 1.0$ °C); a reduction to 5% of P (Run 15) resulted in a further water-table decline and warmer temperatures ($\Delta h = -817$ m, $\Delta T = 11.3$ °C) compared to Run 20 (Fig. 10; Table 5). In order to evaluate a purely conductive heat-flux regime, a no-recharge simulation (Run 45) indicates that temperatures at sea level would range from about 80 °C beneath the caldera to 30 °C at the coast.

Model results are mildly sensitive to variations in basal heat flux (Q_h). Q_h affects the model by modulating background temperatures and influencing K_{sat} through temperature-dependent viscosity; an increase in Q_h effectively decreases viscosity and increases hydraulic conductivity. Based on previously published values (discussed above), Q_h was varied from 0.04 to 1.0 W m⁻². In general, higher values of Q_h cause a reduction in simulated water-table altitude and an increase in aquifer temperatures. For example, simulations with K_{sat} of 10^{-7} m s⁻¹ and R set to 25% of P , doubling Q_h from 0.1 W m⁻² (Run 29) to 0.2 W m⁻² (Run 38) lowered the water table by 53 m beneath the caldera and by 10 m at $x = 8$ km, while increasing water-table temperatures by 0.2–1.0 °C. With a smaller K_{sat} of 3.75×10^{-8} m s⁻¹ and R set to 12% of P , the same doubling of Q_h lowered the water table by 105 m beneath the caldera to 21 m at 8 km, while increasing water-table temperatures by 1.3–1.6 °C (Runs 8 and 34). Setting Q_h to 1 W m⁻² beneath the caldera and 0.1 W m⁻² elsewhere (Run 35) produces a deeper ($\Delta h = -225$ m beneath the caldera and -22 m at 8 km) and warmer ($\Delta T = 10.6$ °C beneath the caldera and 2.3 °C at 8 km) water table compared to a uniform heat flux of 0.1 W m⁻² (Run 8). This suggests that the lower basal heat flux of 0.1 W m⁻² used in the primary series of simulations is reasonable.

Model results are relatively insensitive to values of porosity and thermal conductivity. For a recharge rate of 12% of precipitation, increasing porosity from 0.05/0.10 for BEC/PEC (Run 12) to 0.30 (Run 43) while keeping other parameters constant resulted in only a small increase in water-table altitude beneath the caldera ($\Delta h = 12$ m), and temperatures changed by less than 0.5 °C at all distances. Decreasing thermal conductivity from 2.2 W m⁻¹ °C⁻¹ (runs 3, 27, 29) to 1.0 W m⁻¹ °C⁻¹ (runs 39 through 41) produced mixed results, with only slight decreases in water-table temperature and slight increases in water-table altitude for higher K_{sat}

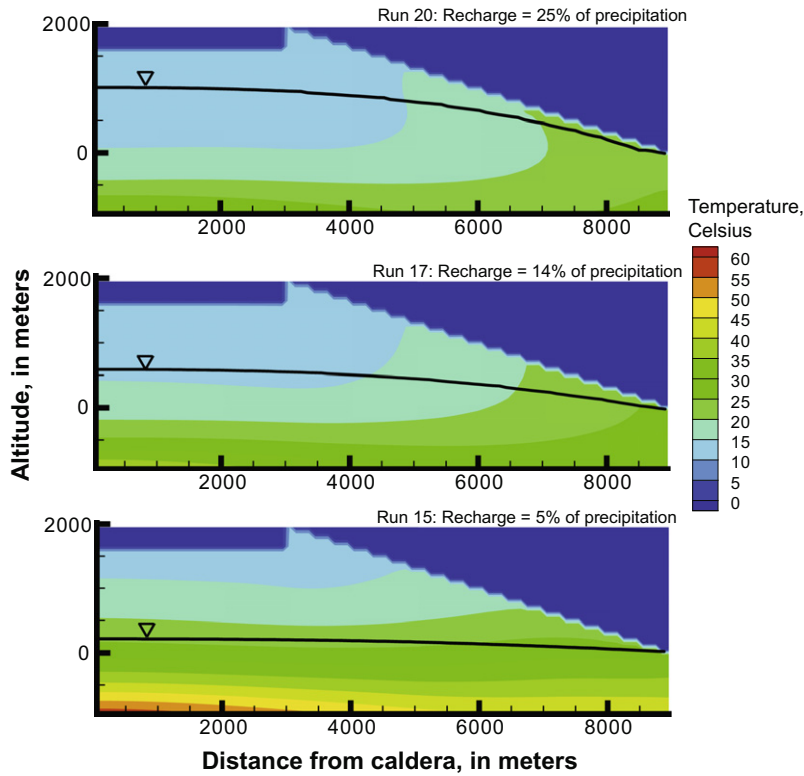


Fig. 10. Comparison of computed temperature and water-table altitudes for simulations with recharge rates of (a) 25%, (b) 14%, and (c) 5% of precipitation.

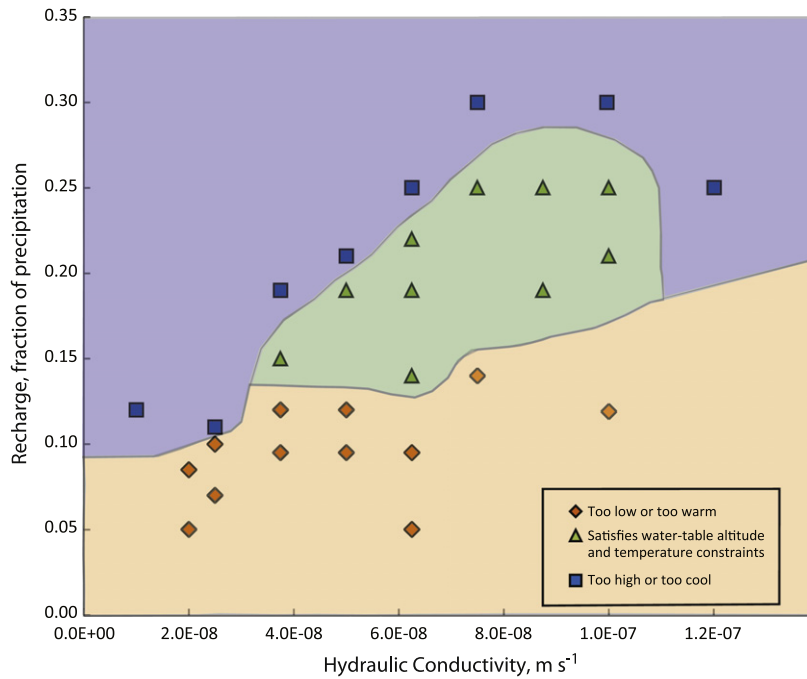


Fig. 11. Solution space for the subset of simulations evaluating varying hydraulic conductivity and recharge rate on water-table altitude and temperature.

(10^{-7} m s^{-1}), yet decreased temperatures and altitudes for lower K_{sat} ($2 \times 10^{-8} \text{ m s}^{-1}$). Temperature at the base of the simulated domain (not shown in Table 5) increased with decreasing thermal conductivity for all three simulations ($\Delta T = 11.8, 7.9,$ and $5.5 \text{ }^\circ\text{C}$ at 0 km for simulations 40 through 42, respectively).

A wide range of recharge rates and hydraulic-conductivity values were tested with the numerical model, but acceptable simulations were obtained for only a relatively narrow range of values.

With a basal heat flux of 0.1 W m^{-2} , thermal conductivity of $2.2 \text{ W m}^{-1} \text{ K}^{-1}$, and PEC and BEC porosity values of 0.10 and 0.05 respectively, permissible K_{sat} values ranged from about 4×10^{-8} to $1 \times 10^{-7} \text{ m s}^{-1}$. These simulated hydraulic conductivity values and recharge rates are at the lower end of the range of reported values for other volcanic islands. The low hydraulic conductivity indicates either bulk matrix permeability lower than typical basalt or the prevalence of low-permeability structures such as dikes.

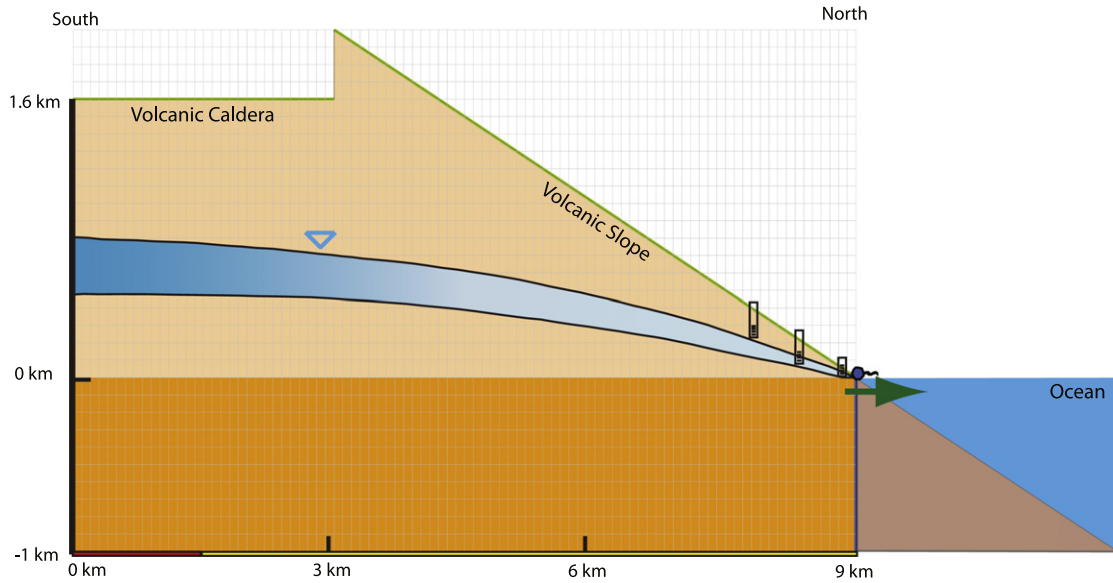


Fig. 12. Diagram showing range of simulated inland water-table altitudes consistent with measured water-table altitude and temperature data.

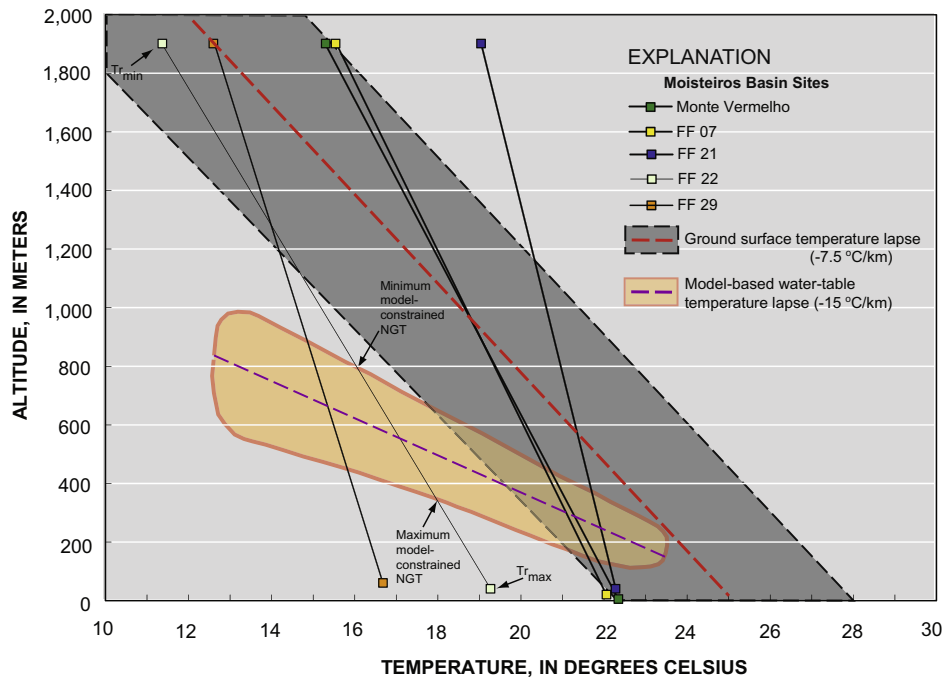


Fig. 13. Temperature lapse bands and the range of possible noble-gas recharge temperatures for groundwater sites in Mosteiros Basin.

Higher hydraulic conductivities require higher recharge fractions, but at some point the system cools and modeled groundwater temperatures become too cold. Simulation results constrain recharge to 12–25% of precipitation (Fig. 11, Table 5), resulting in a weighted average recharge rate along the 9-km transect of the Mosteiros groundwater basin of $70\text{--}140\text{ mm yr}^{-1}$ ($3\text{--}6\text{ Mm}^3\text{ yr}^{-1}$). This range is generally lower than previously reported recharge to volcanic island aquifer systems having similar permeability and topographic slope. The low recharge, both in absolute rates and as a percentage of precipitation, for Mosteiros are likely related to the lower amount of rainfall and drier conditions in Cape Verde compared with other studied volcanic islands having similar permeability and topographic slope (Hawaii, Reunion). Studies have shown that the percentage of recharge declines with precipitation amount (Healy, 2010; Masbruch et al., 2011).

The acceptable simulations produced a range of predicted water-table profiles that are relatively deep beneath the volcanic caldera and upper slope, yet relatively shallow near the coastal aquifer (Fig. 12). Predicted water-table altitudes beneath the center of the caldera floor ($x = 0\text{ km}$) range from about 600 to 1000 m, corresponding to water-table depths below land surface of 1000–600 m; predicted water-table altitudes beneath the caldera wall ($x = 3\text{ km}$) range from about 600 to 900 m, corresponding to water-table depths below land surface of 1400–1100 m; predicted water-table altitudes beneath the upper part of the volcanic slope ($x = 6\text{ km}$) range from about 400 to 600 m, corresponding to water-table depths below land surface of 500–300 m. These simulations are based on a simplified homogenous representation of the aquifer system; further investigation may locate areas of shallower groundwater caused by lower-permeability features such as intru-

sive dikes. Nevertheless, these relatively large simulated depths to groundwater imply that development of upland groundwater resources would involve great expense.

5. Discussion

Recharge temperatures calculated for each noble-gas sample can be constrained by intersection of the Tr_{\min}/Tr_{\max} line with a recharge temperature lapse band. In prior studies, a Tr lapse has been derived either theoretically based on a simple relationship between mean air temperature and shallow ground temperature (e.g., Aeschbach-Hertig et al., 1999) or empirically using discharge temperatures and/or NGTs for springs at various altitudes (e.g., Manning, 2011). While Manning and Solomon (2003) have shown that NGTs in recharge areas with a shallow water table may be a few degrees cooler than spring or mine-tunnel discharge, the slopes of the lapse curves derived from these two data types were similar. The ground-surface temperature lapse band derived for Cape Verde from spring temperatures has a slope of -7.5 °C per km (Fig. 5), whereas numerical model results indicate a water-table lapse rate of -10 to -23 °C per km (Fig. 13). These steeper water-table temperature lapse rates are likely caused by the cooling effect of infiltration of precipitation moving downward through a thick vadose zone. The range of possible NGTs for groundwater samples collected in Mosteiros Basin (11 – 22 °C; Table 4) is based on recharge occurring at any altitude between the sampling site and the maximum possible water-table elevation within the watershed (1900 m). The numerical simulations, however, indicate that maximum water-table altitudes beneath the caldera and upper volcanic slope are in the range of 600–1000 m. When the numerical-model-based water-table temperature lapse band is used, the range of possible NGTs for the Mosteiros Basin is reduced to about 15 – 22 °C, eliminating the cooler end of the NGT range. Individually, the range of possible NGTs for each of the groundwater sites is even further reduced. For example, the range of NGTs for site FF 22 is reduced from about 11 – 19 °C (Table 4) to 16 – 18 °C. Had the spring-based temperature lapse been used instead to constrain NGTs for this site, the resulting range would have been much cooler at 11 to 15 °C. The numerical modeling indicates that water-table temperatures at distances <6 km from the caldera are all in the range of 12 – 14 °C, cooler than the calculated noble-gas recharge temperatures. This implies a significant amount of recharge occurring lower along the volcanic slope where the temperature of infiltrating precipitation is warmer. This important recharge location information could not be determined using only the NGT information.

The numerical simulations of groundwater conditions in Mosteiros Basin indicate recharge rates ranging from 12% to 25% of average annual precipitation, much higher than the measured groundwater discharge of only about 1% of estimated precipitation. This indicates that a substantial amount of discharge from the aquifer may occur as unmeasured submarine outflow. This finding is consistent with previous reports of freshwater discharge to the ocean off of the northern coast of Fogo.

The modeling also indicates that permissible K_{sat} values for Mosteiros Basin range from 4×10^{-8} to 1×10^{-7} m s^{-1} . These K_{sat} values are at the low end of previously published values for ocean island basalts and slightly lower than the range of 10^{-7} to 10^{-6} m s^{-1} determined from hydraulic analysis of aquifer response to dewatering of the Galeria Fajã (Sao Nicolau) during the 1980s. This likely indicates that intrusive dikes or other low-permeability features may be significant in controlling the upland hydrologic system in Mosteiros Basin.

Hydraulic conductivity was assumed to be isotropic for this analysis. Other studies (e.g. Hurwitz et al., 2003) have assumed anisotropy in permeability for volcanic systems. Sensitivity of simulation results to anisotropy shows that decreasing vertical permeability by up to a factor of 10 relative to horizontal permeability resulted in moderately higher water tables but little change in sim-

ulated temperature. Even with this anisotropy, the vertical and horizontal conductivities must fall within the acceptable range of values depicted in Fig. 11 in order to satisfy temperature and water-table altitude constraints. The simple 2-layer isotropic depiction of the aquifer system was invoked in our numerical model partly due to the lack of detailed geologic and hydraulic information for the Mosteiros Basin. Thus, this conceptual/numerical model may not be unique; other representations are possible.

6. Conclusions

The modeling of coupled groundwater flow and heat transport for a volcanic island aquifer shows the utility of this method for evaluating hydrologic parameters including recharge rates, hydraulic conductivity, and inland water-table altitudes. The modeling was largely constrained by (1) maximum possible inferred water-table altitude beneath the central caldera, and (2) measured water-table altitudes and temperatures within 1 km of the coast. While NGT-derived recharge temperatures do not exclusively rule out non-permissible K_{sat} and recharge values, NGTs provide additional support to the other temperature and water-table constraints. A wide range of recharge rates and hydraulic conductivity were tested with the numerical model, but only a subset of values produced results consistent with available water-table altitude and temperature data. Because of the limited amount of available water-level data in the upland part of the aquifer and the uncertainty of recharge estimates, a unique “best-fit” model cannot be obtained. Instead, simulation results are used to bracket ranges of reasonable parameter values resulting in water-table altitudes and temperatures that fit within observation constraints.

Simulations show that the likely depth to groundwater beneath the caldera is between 700 and 1000 m; depth to groundwater beneath the upper slopes of the volcano (between elevations of 1 and 2 km) likely exceeds 500 m. Such depths generally preclude economically feasible development of groundwater resources. Modeling also indicates that relatively cool water-table temperatures of 13 – 15 °C likely occur beneath the central caldera and 17 – 19 °C beneath the upper volcanic slope, resulting in a much steeper water-table lapse (-15 °C/km) than typical adiabatic lapse rates. This is consistent with depressed temperatures to depths of 500 to 1000 m found in deep boreholes in the Kilauea volcanic caldera of Hawaii (Kauahikaua, 1993) and isothermal air temperature measured to depths of 1000 m in boreholes on the flanks of the Newberry volcano of Oregon (Swanberg et al., 1988). Such cool temperatures at great depth confirm the importance of thermal mass transfer via the advective flushing of heat by groundwater circulation, swamping out the warm temperatures at depth that would otherwise exist due to the geothermal gradient in the absence of infiltrating precipitation. This is further supported by the relatively cool noble-gas derived recharge temperatures and measured spring temperatures in Mosteiros Basin. The numerical simulations illustrate conceptually that recharge has a strong cooling effect on aquifer conditions, even in an active volcanic complex having a relatively large basal heat flux, low recharge rates, and a deep upland water table.

Acknowledgements

This work was made possible through funding by the Millennium Challenge Corporation. Data and technical support provided by hydrologists and technicians from the Instituto Nacional de Gestão dos Recursos Hídricos was essential for the completion of this study. The authors thank Niel Plummer (U.S. Geological Survey National Research Program) and D. Kip Solomon (University of Utah Department of Geology and Geophysics) for their insightful discussions and comments, along with Stephen Gingerich (U.S. Geological Survey

Hawaii Water Science Center) and Grant Ferguson (University of Saskatchewan) for their helpful peer reviews. The first author would also like to acknowledge Ingrid Verstraeten (U.S. Geological Survey International Programs Office) for her assistance in the collection of environmental tracer samples and overall project management.

Appendix A

Table A1.

Table A1
Reported hydraulic conductivity values for volcanic island aquifers.

Volcano or Island	State/country	K_{sat} (m/s)	Method	Reference	Comments
Oahu	Hawaii, USA	10^{-12} – 10^{-2}	Aquifer testing	Mink and Lau (1980)	Weathered and nonweathered Ko'olau basalt, lower Waiawa Valley
Oahu	Hawaii, USA	10^{-6} – 10^{-2}	Lab measurements and aquifer testing	Nichols et al. (1996), Table 2	All volcanics including both dike complexes and dike-free basalts
Piton de la Fournaise	La Réunion	10^{-3} – 10^{-1}	Aquifer testing	Violette et al. (1997)	Basaltic lava flows
Madeira Island ^a	Portugal	10^{-5} – 10^{-3}	Aquifer testing	Prada et al. (2005)	Main volcanic complex
Gran Canaria ^a	Canary Islands	10^{-6} – 10^{-4}	Aquifer testing	Cabrera and Custodio (2004)	Pyroclastic deposits, ash-flows and recent basalts
(Summary of 5 islands)	Hawaii, USA	10^{-5} – 10^{-2}	Aquifer testing	Rotzoll and El-Kadi (2008a)	Dike-free basalts
Oahu	Hawaii, USA	10^{-4} – 10^0	Aquifer testing	Hunt (1996)	Summary of reported tests from dike-free basalts
Oahu	Hawaii, USA	10^{-4}	Aquifer testing	Hunt (1996)	Summary of reported tests from dike- <i>i</i> -intruded basalts
Oahu	Hawaii, USA	10^{-3} – 10^{-2}	Aquifer testing	Nichols et al. (1996), Table 3	Dike-free basalts
Maui	Hawaii, USA	10^{-5} – 10^{-2}	Single-well aquifer testing	Rotzoll et al. (2007)	Dike-free basalts
Central Maui	Hawaii, USA	10^{-2}	Wave setup method and numerical modeling	Rotzoll and El-Kadi (2008b)	Regional value for dike-free basalts
Kilauea rift zone ^b	Hawaii, USA	$\geq 10^{-3}$	Numerical modeling/single-well mud-loss rates	Ingebritsen and Scholl (1993)	Unaltered surficial basalts
Kilauea rift zone ^b	Hawaii, USA	$\leq 10^{-8}$	Regional numerical modeling	Ingebritsen and Scholl (1993)	Deeply buried (>1 km) hydrothermally altered basalts

^a Based on transmissivity data and assuming an aquifer thickness of 100 m.

^b Converted from intrinsic permeability.

References

- Aeschbach-Hertig, W., Peeters, F., Beyerle, U., Kipfer, R., 1999. Interpretation of dissolved atmospheric noble gases in natural waters. *Water Resour. Res.* 35, 2779–2792.
- Aeschbach-Hertig, W., Peeters, F., Beyerle, U., Kipfer, R., 2000. Paleotemperature reconstruction from noble gases in ground water taking into account equilibrium with trapped air. *Nature* 405, 1040–1044.
- Anderson, M.P., 2005. Heat as a groundwater tracer. *Groundwater* 43 (6), 951–968.
- Ballentine, C.J., Hall, C.M., 1999. Determining paleotemperature and other variables by using an error-weighted, nonlinear inversion of noble gas concentrations in water. *Geochim. Cosmochim. Acta* 63, 2315–2336.
- Barmen, G., Carvalho, V., Querido, A., 1990. Groundwater-related Geological and Isotopic Investigations on the Island of Fogo: An Overview. Lund University Institute of Tech. Rep. LUTVDG/TVTG-90/3027, 72pp.
- Böhlke, J.K., 2006. TRACERMODEL1. Excel workbook for calculation and presentation of environmental tracer data for simple groundwater mixtures. In: Use of Chlorofluorocarbons in Hydrology, a Guidebook, IAEA STI/PUB/1238. IAEA, Vienna, Austria, pp. 239–243.
- Cabrera, M.C., Custodio, E., 2004. Groundwater flow in a volcanic-sedimentary coastal aquifer: Telde area, Gran Canaria, Canary Islands, Spain. *Hydrogeol. J.* 12 (4), 305–320.
- Chiodini, G.F., Frondini, F., Ponziani, F., 1995. Deep structures and carbon dioxide degassing in central Italy. *Geothermics* 24 (1), 81–94.
- Christensen, B.P., Holm, P.M., Jambon, A., Wilson, J.R., 2001. Helium, argon, and lead isotopic composition of volcanics from Santo Antão and Fogo, Cape Verde Islands. *Chem. Geol.* 178, 127–142.
- Clauser, C., Huenges, E., 1995. Thermal conductivity of rocks and minerals in rock physics and phase relations: a handbook of physical constants. Am. Geophys. Union, 105–126.
- Cook, P.G., Solomon, D.K., 1995. Transport of atmospheric trace gases to the water table: implications for groundwater dating with chlorofluorocarbons and krypton 85. *Water Resour. Res.* 31 (2), 263–270.
- Courtney, R.C., White, R.S., 1986. Anomalous heat flow and geoid across the Cape Verde Rise: evidence for dynamic support from a thermal plume in the mantle. *Geophys. J. R. Astron. Soc.* 87, 815–867.
- Dallai, L., Magro, G., Petrucci, E., Ruggieri, G., 2005. Stable isotope and noble gas isotope compositions of inclusion fluids from Larderello geothermal field (Italy): constraints to fluid origin and mixing processes. *J. Volcanol. Geotherm. Res.* 148, 152–164.
- Deming, D., 2001. Introduction to Hydrogeology. McGraw-Hill, New York.
- Descloîtres, M., Guérin, R., Albouy, Y., Tabbagh, A., Ritz, M., 2000. Improvement in TDEM sounding interpretation in presence of induced polarization. A case study in resistive rocks of the Fogo volcano, Cape Verde Islands. *J. Appl. Geophys.* 45, 1–18.
- Dittrich, I., 1982. Les debits de Projet pour la Zone de Praia et l'Influence d'Urbanisation sur l'Écoulement de Surface. MDR/GEP, Praia, Repub. of Cape Verde.
- Engott, J.A., 2011. A Water-budget Model and Assessment of Groundwater Recharge for the Island of Hawaii. U.S. Geol. Surv. Sci. Investig. Rep. 2011–5078, 53p.
- Engott, J.A., Vana, T.T., 2007. Effects of Agricultural Land-use Changes and Rainfall on Ground-water Recharge in Central and West Maui, Hawaii, 1926–2004. U.S. Geol. Surv. Sci. Investig. Rep. 2007–5103, 56p.
- Fernandez, J., Vieira, R., Diez, J.L., Toro, C., 1992. Investigations on crustal thickness, heat flow and gravity tide relationship in Lanzarote Island. *Phys. Earth Planet. Int.* 74, 199–208.
- Flint, A.L., Flint, L.E., Havesi, J.A., Blainey, J.M., 2004. Fundamental concepts of recharge in the Desert Southwest: a regional modeling perspective. In: Hogan, J.F., Phillips, F.M., Scanlon, B.R. (Eds.), *Groundwater Recharge in a Desert Environment: The Southwestern United States*. Am. Geophys. Union, Water Sci. and Appl. Ser. 9, pp. 159–184.
- Forster, C., Smith, L., 1988. Groundwater flow systems in mountainous terrain: 2. Controlling factors. *Water Resour. Res.* 24 (7), 1011–1023.
- Gingerich, S.B., 1999. Estimating Transmissivity and Storage Properties from Aquifer Tests in the Southern Lihue Basin, Kauai, Hawaii. U.S. Geol. Surv. Sci. Investig. Rep. 99–4066, 33p.
- Gingerich, S.B., Oki, D.S., 2000. Ground Water in Hawaii. U.S. Geol. Surv. Fact Sheet 6, 126–00.
- Harris, R.N., McNutt, M.K., 2007. Heat flow on hot spot swells: evidence for fluid flow. *J. Geophys. Res.* 112 (B03407), 14. <http://dx.doi.org/10.1029/2006JB004299>.
- Harris, R.N., Von Herzen, R.P., McNutt, M.K., Garven, G., Jordahl, K., 2000. Submarine hydrogeology of the Hawaiian archipelagic apron, Part 1. Heat flow patterns north of Oahu and Maro Reef. *J. Geophys. Res.* 105 (21), 21353–21369.

- Healy, R.W., 2010. Estimating Groundwater Recharge. Cambridge University Press, Cambridge, UK, p. 245.
- Healy, R.W., Ronan, A.D., 1996. Documentation of computer program VS2DH for simulation of energy transport in variably saturated porous media: modification of the U. S. Geological Survey's computer program VS2DT. U.S. Geol. Surv. Water-Resour. Invest. Rep. 96–4230.
- Heilweil, V.M., Earle, J.D., Cederberg, J.R., Messer, M.M., Jorgensen, B.J., Verstraeten, I.M., Moura, M.A., Querido, A., Spencer, F., Osorio, T., 2006. Evaluation of Baseline Ground-water Conditions in the Mosteiros, Ribeira Paul, and Ribeira Fajã Basins, Republic of Cape Verde, West Africa, 2005–06. U.S. Geol. Surv. Sci. Investig. Rep. 2006–5207, p. 42.
- Heilweil, V.M., Solomon, D.K., Gingerich, S.B., Verstraeten, I.M., 2009. Oxygen, hydrogen, and helium isotopes for investigating groundwater systems of the Cape Verde Islands, West Africa. *Hydrogeol. J.* 17, 1157–1174.
- Hildenbrand, A., Marlin, C., Conroy, A., Gillot, P.Y., Filly, A., Massault, M., 2005. Isotopic approach of rainfall and groundwater circulation in the volcanic structure of Tahiti-Nui (French Polynesia). *J. Hydrol.* 302, 187–208.
- Horai, K., 1991. Thermal conductivity of Hawaiian basalt: A new interpretation of Roberston and Peck's Data. *J. Geophys. Res.* 96 (B3), 4125–4132.
- Hsieh, P.A., Wingle, W., Healy, R.W., 1999. VS2DI - a graphical software package for simulating fluid flow and solute or energy transport in variably saturated porous media. U.S. Geol. Surv. Water-Resour. Invest. Rep. 99–4130.
- Hunt, C.D., 1996. Geohydrology of the Island of Oahu, Hawaii. U.S. Geol. Surv. Prof. Pap. 1412-B, 54p.
- Hurwitz, S.E., Ingebritsen, S.E., Sorey, M.L., 2002. Episodic thermal perturbations associated with groundwater flow: an example from Kilauea Volcano, Hawaii. *J. Geophys. Res.* 107(B11), 2297. <http://dx.doi.org/10.1029/2001JB001654>.
- Hurwitz, S., Kipp, K.L., Ingebritsen, S.E., Reid, M.E., 2003. Groundwater flow, heat transport, and water table position within volcanic edifices: implications for volcanic processes in the Cascade Range. *J. Geophys. Res.* 108 (B12), 2557. <http://dx.doi.org/10.1029/2003JB002565>.
- Ingebritsen, S.E., Scholl, M.A., 1993. The hydrogeology of Kilauea volcano. *Geothermics* 22, 255–270.
- Ingebritsen, S.E., Sanford, W.E., Neuzil, C.E., 2006. Groundwater in Geologic Processes. Cambridge University Press, Cambridge, 536p.
- Ingebritsen, S.E., Geiger, S., Hurwitz, S., Driesner, T., 2010. Numerical simulation of magmatic hydrothermal systems. *Rev. Geophys.* 48, 2009RG000287, 33p.
- Institut Géographique National de France, 1981. Etude des resurgences d'eau douce par thermographies, République du Cap Vert: Département de télédétection et cartographie spatiale. Ministère de la coopération et du développement économique, 42p.
- Izuka, S.K., Gingerich, S.B., 2003. A thick lens of fresh groundwater in the southern Lihue Basin, Kauai, Hawaii, USA. *Hydrogeol. J.* 11, 240–248.
- Izuka, S.K., Oki, D.S., Chen, C., 2005. Effects of Irrigation and Rainfall Reduction on Ground-water Recharge in the Lihue Basin, Kauai, Hawaii. U.S. Geol. Surv. Sci. Investig. Rep. 2005–5146, p. 48.
- Jackson, D.B., Lenat, J.F., 1989. High-level water tables on Hawaiian type volcanoes and intermediate depth geoelectric structures, Kilauea Volcano, Hawaii and Piton de la Fournaise Volcano, Isle de la Reunion. *N. M. Bur. of Geol. and Miner. Resour.*, pp. 131 and 142.
- Kallrén, L., Schreiber, I., 1988. Groundwater Survey on Western Fogo, Cape Verde. Lund Inst. of Tech. Rep. TVTG-5019, p. 83.
- Kauahikaua, J., 1993. Geophysical characteristics of the hydrothermal systems of Kilauea Volcano, Hawaii. *Geothermics* 22, 271–299.
- Keller, G.V., Trowbridge, G., Murray, J.C., Skokan, C.K., 1979. Results of an experimental drill hole at the summit of Kilauea volcano, Hawaii. *J. Volcanol. Geotherm. Resour.* 5, 345–385.
- Langworthy, M., Finan, T.J., 1997. Waiting for Rain: Agriculture and Ecological Imbalance in Cape Verde. Lynne Rienner Publishers, Boulder, Colo., p. 212.
- Liu, C.C., Lau, L.S., Mink, J.F., 1983. Ground-water model for a thick fresh-water lens. *Groundwater* 21 (3), 293–300.
- MacDonald, G.A., Abbott, A.T., Peterson, F.L., 1983. Volcanoes in the sea: the geology of Hawaii, (second ed.), University of Hawaii Press, Honolulu, Hawaii, 517 p.
- Manning, A.H., 2011. Mountain-block recharge, present and past, in the eastern Espanola Basin, New Mexico, USA. *Hydrogeol. J.* 19 (2), 379–398.
- Manning, A.H., Caine, J.S., 2007. Groundwater noble gas, age, and temperature signatures in an alpine watershed: valuable tools in conceptual model development. *Water Resour. Res.* 43 (W04404), 16. <http://dx.doi.org/10.1029/2006WR005349>.
- Manning, A.H., Solomon, D.K., 2003. Using noble gases to investigate mountain-front recharge. *J. Hydrol.* 275 (3–4), 194–207.
- Masbruch, M.D., Heilweil, V.M., Buto, S.G., Brooks, L.E., Susong, D.D., Flint, A.L., Flint, L.E., Gardner, P.M., 2011. Chapter D: Estimated groundwater budgets. In: Heilweil, V.M., Brooks, L.E. (Eds.), Conceptual Model of the Great Basin Carbonate and Alluvial Aquifer System. U.S. Geol. Surv. Sci. Investig. Rep. 2010–5193, p. 191.
- Mazor, E., 1991. Applied Chemical and Isotopic Groundwater Hydrology. Halsted, NY, p. 274.
- Mazor, E., Verhagen, B.T., 1976. Hot springs of Rhodesia: their noble gases, isotopic and chemical composition. *J. Hydrol.* 28, 29–43.
- Meinzer, O.E., 1930. Ground water in the Hawaiian islands. In: Stearns, H.T., Clark, W.O. (Eds.), Geology and Water Resources of the Kau District, Hawaii: U.S. Geological Survey Water-Supply Paper 616, pp. 1–28.
- Mink, J.F., Lau, S.L., 1980. Hawaiian Groundwater Geology and Hydrology, and Early Mathematical Models. Univ. of Hawaii Tech. Rep. 62, p. 75.
- Natland, J., 1978. Composition of Basaltic Rocks Recovered at Sites 367 and 368 Deep Sea Drilling Project, Near the Cape Verde Islands. Deep Sea Drilling Proj. Initial Rep. 41, 1107–1112. <http://dx.doi.org/10.2973/dsdp.proc.41.145.1978>.
- Nichols, W.D., Shade, P.J., Hunt, C.D., 1996. Summary of the Oahu, Hawaii, Regional Aquifer-System Analysis. U.S. Geol. Surv. Prof. Pap. 1412-A, p. 71.
- Nilson, R.H., Peterson, E.W., Lie, K.H., Burkhard, N.R., Hearst, J.R., 1991. Atmospheric pumping: a mechanism causing vertical transport of contaminated gases through fractured permeable media. *J. Geophys. Res.* 96 (B13), 21933–21948.
- Oki, D.S., 2005. Numerical Simulation of the Effects of Low-Permeability Valley-Fill Barriers and the Redistribution of Ground-Water Withdrawals in the Pearl Harbor Area, Oahu, Hawaii. U.S. Geol. Surv. Sci. Investig. Rep. 2005–5253, p. 111.
- Pim, J., Peirce, C., Watts, A.B., Grevemeyer, I., Krabbenhoft, A., 2008. Crustal structure and the origin of the Cape Verde Rise. *Earth Planet. Sci. Lett.* 272, 422–428.
- Plummer, L.N., Rupert, M.G., Busenberg, E., Schlosser, P., 2000. Age of irrigation water in ground water from the eastern Snake River Plain aquifer, south-central Idaho. *Groundwater* 38 (2), 264–283.
- Powell, W.G., Chapman, D.S., Balling, N., Beck, A.E., 1988. Continental heat-flow density. In: Haenel, R., Ryback, L., Stegena, L. (Eds.), Handbook of Terrestrial Heat-Flow Density Determination with Guidelines and Recommendations of the International Heat Flow Commission. Kluwer Acad. Publ., Boston, pp. 167–222.
- Prada, S.N., da Silva, M.O., Cruz, J.V., 2005. Groundwater behavior in Madeira, volcanic island (Portugal). *Hydrogeol. J.* 13 (5–6), 800–812.
- Putnam, S.N., Chapman, D.S., 1996. A geothermal climate change observatory: first year results from Emigrant Pass in northwest Utah. *J. Geophys. Res.* 101, 21877–21890.
- Rotzoll, K., El-Kadi, A.I., 2008a. Estimating hydraulic conductivity from specific capacity for Hawaii aquifers, USA. *Hydrogeol. J.* 16, 969–979.
- Rotzoll, K., El-Kadi, A.I., 2008b. Estimating hydraulic properties of coastal aquifers using wave setup. *J. Hydrol.* 353, 201–213.
- Rotzoll, K., El-Kadi, A.I., Gingerich, S.B., 2007. Estimating hydraulic properties of volcanic aquifers using constant-rate and variable-rate aquifer tests. *J. Am. Water Resour. Assoc.* 43 (2), 334–345.
- Sabino, A.A., Querido, A.L., Sousa, M.I., 1999. Flood management in Cape Verde. The case study of Praia. *Urban Water* 1, 161–166.
- Sheldon, A., 2002. Diffusion of Radiogenic Helium in Shallow Ground Water: Implications for Crustal Degassing. PhD Dissertation, Univ. of Utah, Utah, 185p.
- Silva, L.C., Serralheiro, A., Torres, P.C., Mendes, M.H., 2004. Geology of Recent Volcanic Formations from Santo Antão Island, Cape Verde. 20th Colloquium African Geol. Abstr., 378, Orleans.
- Stein, C., Stein, S., 1992. A model for the global variation in oceanic depth and heat flow with lithospheric age. *Nature* 359, 123–129. <http://dx.doi.org/10.1038/359123a0>.
- Stein, C.A., Von Herzen, R.P., 2007. Potential effects of hydrothermal circulation and magmatism on heatflow at hotspot swells. *Geol. Soc. Am. Spec. Pap.* 430 (13), 261–274. <http://dx.doi.org/10.1130/2007.2430>.
- Stute, M., Schlosser, P., 2001. Atmospheric noble gases. In: Cook, P.G., Herczeg, A.L. (Eds.), Environmental Tracers in Subsurface Hydrology. Kluwer Acad. Publ., Boston, Mass., pp. 349–377.
- Swanberg, C.A., Walkley, W.C., Combs, J., 1988. Core hole drilling and the “rain curtain” phenomenon at Newberry volcano, Oregon. *J. Geophys. Res.* 93 (10), 163–173.
- Takasaki, K.J., Mink, J.F., 1985. Evaluation of Major Dike-impounded Ground-water Reservoirs, Island of Oahu. U.S. Geol. Surv. Water Supply Paper 2217, p. 77.
- Vailleux, Y., Bourguet, L., 1974. La mise en valeur des eaux souterraines dans l'archipel du Cap Vert. BURGEAP, Ministerio da Coordenação interterritorial, Brigada de Aguas Subterranas do Cabo Verde Final Mission Rep. 140, p. 291.
- Valentin, A., Albert-Beltran, J.F., Diez, J.L., 1990. Geochemical and geothermal constraints on magma bodies associated with historic activity, Tenerife (Canary Islands). *J. Volcanol. Geotherm. Res.* 44, 264–290.
- Violette, S., Ledoux, E., Goblet, P., Carbonnel, J.P., 1997. Carbonnel, J.P., 1997. Hydrologic and thermal modeling of an active volcano: the Piton de la Fournaise, Reunion. *J. Hydrol.* 191, 37–63.
- Von Herzen, R.P., Detrick, R.S., Crough, S.T., Fang, C., 1982. Thermal origin of the hot spot swells: heat flow evidence and thermal models. *J. Geophys. Res.* 87, 6711–6723.
- Weeks, E.P., Earp, D.E., Thompson, G.M., 1982. Use of atmospheric fluorocarbons F-11 and F-12 to determine the diffusion parameters of the unsaturated zone in the southern high plains of Texas. *Water Resour. Res.* 18 (5), 1365–1378.
- Weiss, R.F., 1968. Piggyback sampler for dissolved gas studies on sealed water samples. *Deep-Sea Res.* 15, 695–699.
- Wood, S.A., 2006. Rare earth element systematics of acidic geothermal waters from Taupo Volcanic Zone, New Zealand. *J. Geochem. Explor.* 89 (1–3), 424–427.